UC Irvine

UC Irvine Previously Published Works

Title

Instrument intercomparison of glyoxal, methyl glyoxal and NO2 under simulated atmospheric conditions

Permalink

https://escholarship.org/uc/item/0nw8r4br

Journal

Atmospheric Measurement Techniques, 8(4)

ISSN

1867-1381

Authors

Thalman, R
Baeza-Romero, MT
Ball, SM
et al.

Publication Date

2015

DOI

10.5194/amt-8-1835-2015

Copyright Information

Peer reviewed

Atmospheric
Measurement
Techniques

Instrument intercomparison of glyoxal, methyl glyoxal and NO$_2$ under simulated atmospheric conditions

R. Thalman[1,2,*], M. T. Baeza-Romero[3], S. M. Ball[4], E. Borrás[5], M. J. S. Daniels[4], I. C. A. Goodall[4], S. B. Henry[6], T. Karl[7,8], F. N. Keutsch[6], S. Kim[7,9], J. Mak[10], P. S. Monks[4], A. Muñoz[5], J. Orlando[7], S. Peppe[11], A. R. Rickard[12,**], M. Ródenas[5], P. Sánchez[5], R. Seco[7,9], L. Su[10], G. Tyndall[7], M. Vázquez[5], T. Vera[5], E. Waxman[1,2], and R. Volkamer[1,2]

[1]Department of Chemistry and Biochemistry, University of Colorado Boulder, Boulder, CO, USA
[2]Cooperative Institute for Research in Environmental Sciences (CIRES), Boulder, CO, USA
[3]Escuela de Ingeniería Industrial de Toledo, Universidad de Castilla la Mancha, Toledo, Spain
[4]Department of Chemistry, University of Leicester, Leicester, LE1 7RH, UK
[5]Instituto Universitario UMH-CEAM, Valencia, Spain
[6]Department of Chemistry, University of Wisconsin, Madison, WI, USA
[7]National Center for Atmospheric Research, Boulder, CO, USA
[8]Institute for Meteorology and Geophysics, University of Innsbruck, Innsbruck, Austria
[9]Department of Earth System Science, University of California Irvine, Irvine, CA, USA
[10]School of Marine and Atmospheric Sciences, State University of New York, Stony Brook, NY, USA
[11]School of Earth and Environment, University of Leeds, Leeds, UK
[12]National Centre for Atmospheric Science, School of Chemistry, University of Leeds, Leeds, UK
*now at: Brookhaven National Laboratory, Upton, NY, USA
**now at: National Centre for Atmospheric Science, Wolfson Atmospheric Chemistry Laboratories, Department of Chemistry, University of York, York, UK

Correspondence to: R. Volkamer (rainer.volkamer@colorado.edu)

Abstract. The α-dicarbonyl compounds glyoxal (CHOCHO) and methyl glyoxal (CH$_3$C(O)CHO) are produced in the atmosphere by the oxidation of hydrocarbons and emitted directly from pyrogenic sources. Measurements of ambient concentrations inform about the rate of hydrocarbon oxidation, oxidative capacity, and secondary organic aerosol (SOA) formation. We present results from a comprehensive instrument comparison effort at two simulation chamber facilities in the US and Europe that included nine instruments, and seven different measurement techniques: broadband cavity enhanced absorption spectroscopy (BBCEAS), cavity-enhanced differential optical absorption spectroscopy (CE-DOAS), white-cell DOAS, Fourier transform infrared spectroscopy (FTIR, two separate instruments), laser-induced phosphorescence (LIP), solid-phase micro extraction (SPME), and proton transfer reaction mass spectrometry (PTR-ToF-MS, two separate instruments; for methyl glyoxal only because no significant response was observed for glyoxal). Experiments at the National Center for Atmospheric Research (NCAR) compare three independent sources of calibration as a function of temperature (293–330 K). Calibrations from absorption cross-section spectra at UV-visible and IR wavelengths are found to agree within 2 % for glyoxal, and 4 % for methyl glyoxal at all temperatures; further calibrations based on ion–molecule rate constant calculations agreed within 5 % for methyl glyoxal at all temperatures. At the European Photoreactor (EUPHORE) all measurements are calibrated from the same UV-visible spectra (either directly or indirectly), thus minimizing potential systematic bias. We find excellent linearity under idealized

conditions (pure glyoxal or methyl glyoxal, $R^2 > 0.96$), and in complex gas mixtures characteristic of dry photochemical smog systems (o-xylene/NO$_x$ and isoprene/NO$_x$, $R^2 > 0.95$; $R^2 \sim 0.65$ for offline SPME measurements of methyl glyoxal). The correlations are more variable in humid ambient air mixtures (RH > 45 %) for methyl glyoxal ($0.58 < R^2 < 0.68$) than for glyoxal ($0.79 < R^2 < 0.99$). The intercepts of correlations were insignificant for the most part (below the instruments' experimentally determined detection limits); slopes further varied by less than 5 % for instruments that could also simultaneously measure NO$_2$. For glyoxal and methyl glyoxal the slopes varied by less than 12 and 17 % (both 3-σ) between direct absorption techniques (i.e., calibration from knowledge of the absorption cross section). We find a larger variability among in situ techniques that employ external calibration sources (75–90 %, 3-σ), and/or techniques that employ offline analysis. Our intercomparison reveals existing differences in reports about precision and detection limits in the literature, and enables comparison on a common basis by observing a common air mass. Finally, we evaluate the influence of interfering species (e.g., NO$_2$, O$_3$ and H$_2$O) of relevance in field and laboratory applications. Techniques now exist to conduct fast and accurate measurements of glyoxal at ambient concentrations, and methyl glyoxal under simulated conditions. However, techniques to measure methyl glyoxal at ambient concentrations remain a challenge, and would be desirable.

1 Introduction

The α-dicarbonyl compounds, specifically glyoxal (CHO-CHO, GLY) and methyl glyoxal (CH$_3$C(O)CHO, MGLY), are produced in the atmosphere by the oxidation of hydrocarbons from biogenic (isoprene), anthropogenic (toluene, xylenes, acetylene) and pyrogenic sources (Volkamer et al., 2007; Fu et al., 2008; Myriokefalitakis et al., 2008; Stavrakou et al., 2009; Washenfelder et al., 2011). Time resolved measurements indicate the rate of hydrocarbon oxidation (Volkamer et al., 2005a), and provide information about oxidative capacity (Huisman et al., 2011). Glyoxal and methyl glyoxal are further building blocks that actively participate in the formation of secondary organic aerosol (SOA) in aqueous aerosol particles (Volkamer et al., 2007, 2009; Ervens et al., 2008; Galloway et al., 2009; Hennigan et al., 2009; Ervens and Volkamer, 2010; Hamilton et al., 2013) and cloud droplets (Nozière et al., 2008; Yu et al., 2011; McNeill et al., 2012; Topping et al., 2013). Recent findings also show that the uptake of glyoxal is enhanced by the presence of some inorganic salts (Kampf et al., 2013). SOA formation from the uptake and multiphase chemistry of small oxygenated molecules is receiving increasing attention in recent years, and could be an important pathway to explain elevated field observations of high oxygen-to-carbon ratios in ambient or-

ganic aerosol that cannot be explained by traditional SOA formation mechanisms (Waxman et al., 2013).

Glyoxal and methyl glyoxal measurements have been conducted for almost 30 years (Tuazon and Atkinson, 1990a; Yu et al., 1997), but sensitive and robust in situ techniques suitable to measure these compounds with high time resolution as part of field observations have only become available over the past decade (Volkamer et al., 2005a; Washenfelder et al., 2008; Huisman et al., 2008; Thalman and Volkamer, 2010; Baidar et al., 2013; Henry et al., 2012; DiGangi et al., 2012; Ahlm et al., 2012). Methods span a variety of analytical techniques, in particular the following: infrared (IR) absorption spectroscopy (Tuazon and Atkinson, 1990b; Profeta et al., 2011), ultraviolet-visible (UV-vis) absorption spectroscopy (Volkamer et al., 2005a; Sinreich et al., 2007; Washenfelder et al., 2008; Thalman and Volkamer, 2010), chromatographic analysis of derivatization by O-(2,3,4,5,6-pentafluorobenzyl)-hydroxylamine (PFBHA) (Bao et al., 1998; Ho and Yu, 2002; Baker et al., 2005; Ip et al., 2009; Alvarez and Valcárcel, 2009; Pang et al., 2013, 2014) or DNPH (Grosjean et al., 1996) via C-18 packed columns or solid-phase micro-extraction and detection by mass spectrometry or flame ionization, phosphorescence (Huisman et al., 2008; Henry et al., 2012); and in the case of methyl glyoxal also chemical ionization mass spectrometry (using H$_3$O$^+$, O$_2^+$ or NO$^+$ reagent ions; de Gouw et al., 2003; Michel et al., 2005; Guimbaud et al., 2007; Karl et al., 2009). To our knowledge there has been no previous systematic effort to compare multiple techniques for quantifying α-dicarbonyls under conditions that resemble the polluted urban or pristine atmosphere. Furthermore, there are several methods and conventions to report detection limits for the different instruments in the literature, which complicates a direct comparison between instruments. This work addresses these issues of common language for limits of detection, assesses some likely measurement interferences, calibration standards and general instrument performance in a series of simulation chamber experiments carried out at the National Center for Atmospheric Research (NCAR) reaction chamber in Boulder, Colorado, USA and the Instituto Universitario Universitas Miguel Hernandez-Centro de Estudios Ambientales del Mediterraneo (UMH-CEAM) European Photoreactor (EUPHORE) in Valencia, Spain.

2 Instrumentation and experimental conditions

2.1 Instruments

The various instruments used at both the NCAR and EUPHORE facility are listed in Table 1, and described in the following subsections in more detail. To ensure consistency, all visible absorption instruments used the same literature cross sections for the retrieval of glyoxal (Volkamer et al., 2005b), methyl glyoxal (Meller et al., 1991), NO$_2$ (Vandaele et al.,

Table 1. Instrumentation and measured species at NCAR and EUPHORE.

Instrument[a]	Participant[b]	Location	Measured species[c]	Measured quantity	Sample location
CE-DOAS	CU	NCAR	G,M, N	[d]	Outside
NCAR FTIR	NCAR	NCAR	G, M, N	[d]	Inside
PTR-ToF-MS	NCAR	NCAR	M	[e]	Outside
CE-DOAS	CU	EUPHORE	G, M, N	[d]	Outside Edge
BBCEAS	Leic	EUPHORE	G, M, N	[d]	Center
PTR-ToF-MS	Leic	EUPHORE	M	[e]	Outside Edge
Mad-LIP	UW	EUPHORE	G, M	[d]	Outside Edge
W-DOAS	CEAM	EUPHORE	G, M, N	[d]	Inside
EUPHORE FTIR	CEAM	EUPHORE	G, M	[d]	Inside
SPME/GC-FID	CEAM	EUPHORE	G, M	[e]	Outside Edge

[a] Abbreviations given in the text. [b] Participants (CU – University of Colorado Boulder, USA; NCAR – National Center for Atmospheric Research, Boulder, CO, USA; Leic – University of Leicester, UK; CEAM – CEAM, Spain). [c] G – glyoxal (GLY), M – methyl glyoxal (MGLY), N – NO$_2$. [d] Concentration (molecule cm^{-3}). [e] Volume mixing ratio referenced to temperature and pressure of the chamber as measured in the chamber.

2002), O$_4$ (Hermans et al., 1999; Hermans, 2010) and water vapor (Rothman et al., 2009). A further discussion of the infrared cross sections used by the instruments at the two different facilities is discussed in their respective descriptions and in Sect. 4.1.

2.1.1 NCAR Fourier Transform Infrared Spectrometer (FTIR)

The FTIR instrument is integrated as part of the NCAR chamber, and measures along the long-axis of the chamber (2 m long, 16 passes, giving a total light path of 32 m). The spectrometer consists of a BOMEM DA3.01 FTIR, and was operated at 1 cm^{-1} resolution and collected and averaged 200 spectra between 800 and 4000 cm^{-1} over a period of 4 min. Standard spectra used for spectral subtraction were obtained using the same conditions as above, from scans of samples prepared via injection of known quantities of analyte into the chamber. Absorption cross sections quoted are derived from these standard spectra.

2.1.2 NCAR proton transfer reaction time of flight mass spectrometer (PTR-ToF-MS)

The NCAR chamber experiment involved measurements of VOCs by using a high resolution PTR-ToF-MS (Ionicon Analytik GmbH, Innsbruck, Austria; Jordan et al., 2009). For a detailed review of the instrumentation, refer to de Gouw and Warneke (2007). During the experiment, the PTR-ToF-MS was operated under H$_3$O$^+$ mode, which uses hydronium ions (H$_3$O$^+$) as the primary reagent ions to protonate VOC species. The ionization conditions in the drift tube were controlled by setting the drift voltage at 542 V, drift temperature at 60 °C and drift pressure at 2.3 mbar, resulting in an E/N value of about 120 Td (with E being the electric field strength, and N the gas number density; 1 Td = 10^{-17} V cm^2). The integration time was set to

1 s. A 1/16 inch OD capillary PEEK inlet ($\sim$ 1 m length) heated to 60 °C was used as a transfer line, with a flow rate of 100 standard cm^3 min^{-1}. The transfer line was connected to an unheated 1/8 inch OD PTFE line ($\sim$ 1 m length), which was connected to the chamber outlet through a dilution system. Standard gas calibration was performed by using a custom built calibration system. Zero air was produced by pumping ambient air through a catalytic convertor heated to 400 °C. A gravimetrically prepared gas standard containing isoprene (7.25 ppmv) and camphene (4.87 ppmv) was dynamically diluted by the zero air and analyzed by the PTR-ToF-MS.

2.1.3 University of Colorado light-emitting diode cavity-enhanced differential optical absorption spectrometer (CE-DOAS)

The University of Colorado, Boulder, light-emitting diode Cavity Enhanced Differential Optical Absorption Spectrometer (CE-DOAS) consists of a high-power blue Light Emitting Diode (LED) coupled to a high finesse optical cavity (highly reflective mirrors, measured $R = 0.999972$ at 460 nm, cavity length, $d_0 = 92$ cm, useable range 430–490 nm, corresponding to an absorption path of 18.4 km in dry air; Thalman and Volkamer, 2010). The CE-DOAS instrument was present for both the experiments at NCAR as well as those at EUPHORE and is here used as the comparative standard for purposes of cross-comparison. In the NCAR experiments 5 standard cm^3 min^{-1} of sample flow was sampled from the chamber through a mass flow controller (MKS) and diluted with 500 standard cm^3 min^{-1} of dry air before flowing through the optical cavity. At EUPHORE, the same CE-DOAS setup was connected directly to the chamber. The instrument sampled at 500 standard cm^3 min^{-1} from the chamber without dilution through 1 m long Teflon tubing with a 1 µm size 25 mm diameter Teflon filter (Pall) in a Teflon filter holder (Entegris) at the begin-

Table 2. Overview and description of experiments at NCAR (N) and EUPHORE (E.)

Exp. #	Date	Experiment name	Description
N1	14 Jan 2011	Hydroxyacetone (HACET) + Cl	Methyl glyoxal comparison at 295 K
N2	14 Jan 2011	C$_2$H$_2$ + Cl	Glyoxal comparison at 295 K
N3	14 Jan 2011	C$_2$H$_2$ + OH	Glyoxal comparison at 295 K
N4	2 Feb 2011	HACET + Cl	Methyl glyoxal comparison at 295 K
N5	4 Feb 2011	HACET + Cl	Methyl glyoxal comparison at 295 K
N6	9 Mar 2012	C$_2$H$_2$ + Cl	Glyoxal comparison at 295 K
N7	9 Mar 2012	HACET + Cl	Methyl glyoxal comparison at 295 K
N8	22 Mar 2012	HACET + Cl	Methyl glyoxal comparison at 320 K
N9	22 Mar 2012	C$_2$H$_2$ + Cl	Glyoxal comparison at 320 K
E1[a]	24 Jun 11	Glyoxal intercomparison	Injection of 40 pbbv of glyoxal followed by dilution to 10s of pptv
E2[a]	27 Jun 2011	Methyl Glyoxal intercomparison	Injection of 20 ppbv of methyl glyoxal followed by sequential dilution to 100 pptv
E3[b]	28 Jun 2011	*o*-xylene oxidation	photo-oxidation of *o*-xylene
E4[b]	29 Jun 2011	Isoprene, High NO$_x$	In situ generation of products of isoprene oxidation under high-NO$_x$ conditions. OH production by photolysis of injected HONO.
E5[b]	30 Jun 2011	O$_3$ (A); O$_3$ + C$_2$H$_2$ (B)	(A) Chamber (Teflon) plus ozone and line residence times (B) In situ generation of glyoxal from the reaction of OH + acetylene (OH from TME + O$_3$) in the presence of ozone in the dark
E6[b]	1 Jul 2011	Ambient Air	Ambient Air filling the chamber followed by addition of NO$_x$ and Isoprene (80 µL)
E7[b]	4 Jul 2011	Isoprene, NO$_x$ Control	Repeat of E4 with NO$_x$ control working and lower initial isoprene to keep at lower NO$_x$ levels in the chamber
E8a[a]	5 Jul 2011	Glyoxal Intercomparison	Repeat of Exp 1
E8b[a]	5–6 Jul 2011	Glyoxal overnight dilution	Injection of 55 ppbv glyoxal and dilution overnight
E9[a]	6 Jul 2011	NO$_2$ interference with glyoxal	Addition of 10–200 ppbv of NO$_2$ on top of ∼ 300 pptv glyoxal
E10[a]	6 Jul 2011	NO$_2$ interference with Methyl Glyoxal	Repeat of E9 with the addition of 10–200 ppbv of NO$_2$ on top of ∼ 5 ppbv methyl glyoxal

[a] Experiments with injection of glyoxal or methyl glyoxal; [b] experiments with in situ production of glyoxal/methyl glyoxal.

ning of the line to remove aerosol. Spectra were acquired for 1 min and evaluated against a 5-min reference spectrum in pure nitrogen.

Analysis of CE-DOAS spectra was performed for the retrieval of glyoxal, methyl glyoxal, NO$_2$ and O$_4$ as described in Thalman and Volkamer (2010). The mirror reflectivity was calibrated from the differential Rayleigh scattering of helium and nitrogen (Washenfelder et al., 2008) using the Rayleigh scattering cross-section values as described in Thalman et al. (2014). The mirror reflectivity curve was then used to calculate the absorption path in the cavity using the following equation:

$$L(\lambda) = \qquad\qquad\qquad\qquad\qquad\qquad (1a)$$

$$\frac{d_s}{1 - R(\lambda) + \alpha_{\mathrm{Ray}}^{\mathrm{Air}}(\lambda)d_0 + \sigma_{O_4}(\lambda)N_d^2 O_{2,\mathrm{mixing,ratio}}^2 d_s + \sigma_i(\lambda)c_i d_s}.$$

If this equation is evaluated at 477 nm, knowledge of the O$_2$ volume mixing ratio and cavity pressure confirm control over cavity alignment and R(477 nm) by measuring of the O$_4$

SCD under atmospheric conditions:

$$L(477\,\mathrm{nm}) = \frac{O_{4_{\mathrm{SCD}}}}{N_d^2 O_{2,\mathrm{mixing,ratio}}^2}, \qquad (1b)$$

where $L(\lambda)$ is the effective path length with respect to wavelength (cm), d_s is the sample length (cm), $R(\lambda)$ is the mirror reflectivity with respect to wavelength, α is the extinction due to the Rayleigh scattering in air (cm^{-1}), d_0 is the cavity length (cm), σ_i is the absorption cross section of the corresponding gas, N$_d$ is the density (molecules cm^{-3}), c_i is the concentration of the corresponding gas (molecules cm^{-3}), and O$_{4SCD}$ is the slant column density (concentration × pathlength of O$_4$, cm^{-5} molecule^2). Absorption cross sections are scaled by a wavelength dependant scaling factor based on the path length, that is close to unity and normalized relative to a single wavelength to account for the wavelength dependence, as is described in detail in Thalman and Volkamer (2010). The Windoas software (Fayt and Van Roosendael, 2001) was used to adjust literature cross sections to the instrument resolution, and perform DOAS fitting of multiple reference spectra simultane-
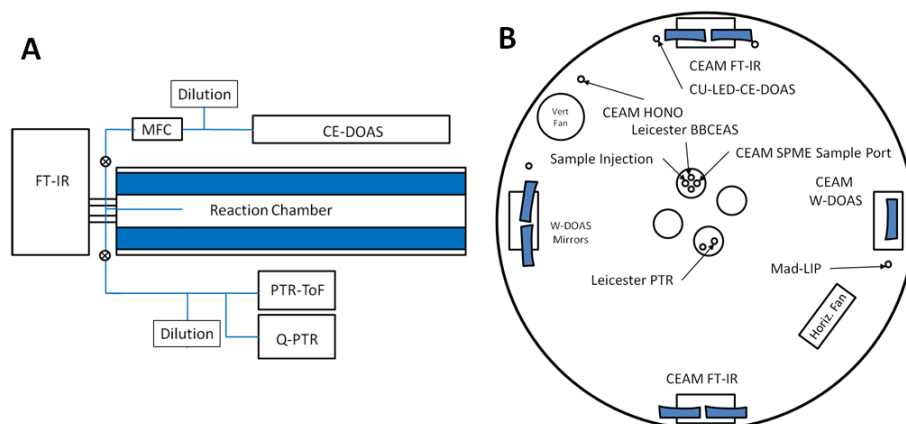
Figure 1. Layout of instruments at NCAR **(a)** and EUPHORE **(b)**. In **(b)** small circles indicate sampling ports; the EUPHORE FTIR, W-DOAS and NCAR-FTIR light paths cross the entire chamber, while other instruments draw air from the chamber for analysis below/outside the chamber.

ously. Glyoxal, methyl glyoxal, NO$_2$, H$_2$O and O$_4$ were retrieved by non-linear least squares fitting (O$_4$ fit window: 457–487 nm, 4th order polynomial; glyoxal fit window: 442–465 nm, 4th order polynomial and Greenblatt et al. (1990) for O$_4$ in this window (see discussion of σ_{O4} baseline noise in Thalman and Volkamer, 2013); glyoxal weak band fit: 458.5–475 nm, 4th order polynomial). The DOAS output in units of slant column density (SCD = concentration × L) was then divided by the path length to get concentration. Measurements of O$_4$ SCDs as part of each spectrum at high signal-to-noise facilitate online control over cavity alignment and/or R. The path length calculated from Eq. (1) agreed with the O$_4$ calibration gas within 1 %. Equation (1) was solved iteratively to account for self-limitation until the concentrations converge. NO$_2$ was self-limiting during E3, E4, E7, E9 and E10 and glyoxal during E1 and E8. For experiments with high glyoxal concentrations, data were retrieved in two ways: (1) fitting of two cross sections bounding the absorption range or (2) fitting of the weak absorption structures in the wavelength range 458.5–475 nm. For experiments N3, E9 and E10 (see Table 2) a NO$_2$ residual is fitted to account for systematic structures arising from extremely high NO$_2$ concentrations leading to a more stable retrieval of the glyoxal or methyl glyoxal concentrations.

2.1.4 University of Leicester broadband cavity-enhanced absorption spectrometer (BBCEAS)

The University of Leicester broadband cavity-enhanced absorption spectroscopy (BBCEAS) instrument is based on predecessor BBCEAS instruments used to detect NO$_2$ in urban air (Langridge et al., 2008) and iodine in the marine atmosphere (Ball et al., 2010). In its present form, it has been deployed as the reference instrument for glyoxal and methyl glyoxal quantification in experiments at

the EUPHORE chamber to test a micro-fluidic derivatisation instrument (Pang et al., 2014) and to investigate glyoxal uptake onto ammonium sulphate aerosol (Hamilton et al., 2013). The instrument uses a high power LED peaking around 455 nm to pump an optical cavity constructed from two high reflectivity plano-concave mirrors separated by 110.5 cm (measured peak reflectivity = 0.999817 at 462 nm, light paths of 5 km when flushed with dry nitrogen). Gas mixtures were sampled from the EUPHORE chamber into the cavity through a PFA inlet line (1.2 m length, 6.35 mm outside diameter, 2 L min^{-1} flow rate) that passed through a bulkhead compression fitting in a flange in the chamber floor, close to the centre of the chamber (see Fig. 1b). The inlet line protruded 40 cm above the chamber floor in order to sample well-mixed gas. Because the BBCEAS instrument shared the same flange used to inject samples into the chamber, the instrument often measured elevated trace gas concentrations during and shortly after injections. Hence data within 5 min of any such trace gas injection have been excluded from the comparisons in this paper.

Spectra of the light intensity transmitted through the cavity and gas sample were recorded using a miniature spectrometer (Ocean Optics HR2000) housed inside a temperature stabilised enclosure. For this work, spectra were integrated for 10 s, and six spectra were averaged together and combined with $I_0(\lambda)$ reference spectra (obtained whilst flushing the cavity with dry synthetic air; averaged for 10 min) to produce BBCEAS spectra at a 1 min time resolution. Absorber concentrations were retrieved by fitting the molecular absorption features in the spectra between 430 and 486 nm using the same reference absorption cross sections as the other spectroscopic instruments (references in Sect. 2.1). Spectra were routinely fitted for glyoxal, methyl glyoxal, NO$_2$, oxygen O$_2$–O$_2$ collision complex and a high order polynomial function (typically 6th order) to account for all remaining unstructured extinction contributions, such as extinction by

secondary organic aerosol formed from VOC oxidation in the EUPHORE chamber. Spectra were also fitted for water absorption bands whenever water vapor had been admitted into the chamber (e.g., the ambient air experiment E6). The highly structured glyoxal, NO$_2$ and water cross sections (Rothman et al., 2009) were degraded to the instrument's spectral resolution (between 0.09 and 0.13 nm half width at half maximum) using asymmetric line shape functions deduced at some 20 wavelengths across the spectrometer's bandwidth by recording and fitting atomic emission lines from argon and krypton calibration lamps. Spectra were not explicitly fitted for ozone or biacetyl absorption, even for experiments where these species were known to be present (see Sect. 4.3); both these molecules have broad, relatively unstructured absorptions within the instrument bandwidth, and their absorptions were adequately fitted by the polynomial function.

Allan variance tests conducted on a long time series of BBCEAS spectra obtained whilst flushing the cavity with dry nitrogen showed that the measurement precision is dominated by random noise components for averaging times up to several hundred seconds. The instrument was subject to small long-term drifts over the ~ 12 h duration of the Allan tests that degraded the achievable precision. However these drifts were always smaller than the 1σ measurement precision for each molecular absorber for the 1 min averaging time, as also evidenced by the modest departures of the BBCEAS data's means from zero in the histograms in Figs. 9 and 10 below. For this deployment at the EUPHORE facility, $I_0(\lambda)$ reference spectra were obtained only at the start and the end of each experiment, whereas more frequent re-acquisitions of the reference spectra during experiments themselves, at time intervals informed by the Allan tests, would reduce the effects of instrument drift. The overall accuracy of the BBCEAS concentration measurements is estimated to be 7 % for glyoxal and NO$_2$ and 10 % for methyl glyoxal. Three main factors (which are comparable in size) control the accuracy: uncertainties in the reference absorption cross sections used to fit the molecular absorbers, uncertainties in determining the reflectivity of the cavity mirrors (this work used a combination of Rayleigh scattering in helium and nitrogen, and absorption by the O$_2$–O$_2$ dimer in pure oxygen samples), and uncertainties in determining the proportion of the cavity occupied by the gas sample (the cavity mirrors were flushed with synthetic air to prevent degradation of the mirror reflectivity during experiments). Daniels and Ball (2015) provide a full discussion of the BBCEAS instrument and its performance.

2.1.5 University of Leicester proton transfer reaction mass spectrometer (PTR-ToF-MS)

A PTR-ToF-MS instrument (Series I, Kore, UK) was employed to detect methyl glyoxal during the EUPHORE experiments. The PTR-ToF-MS technique is based on the chemical ionization of trace VOCs present in atmospheric samples by proton transfer reactions with the hydronium reagent ion (H$_3$O$^+$) (Blake et al., 2009). The product is a protonated molecular ion (VOC-H)$^+$ for each VOC of suitable proton affinity which is then separated and quantified by time-of-flight mass spectrometry (Wyche et al., 2007; Blake et al., 2009)

The PTR-ToF-MS method can also measure oxygenated VOCs such as glyoxal and methyl glyoxal. However, one drawback to PTR-ToF-MS, common to mass spectrometric techniques, is isobaric interference between VOC species being sampled; glyoxal is isobaric with acetone and propanal while methyl glyoxal is isobaric with several oxidized C$_4$ species and also the protonated water cluster (H$_2$O)$_4\cdot$H$^+$. A full discussion of the challenges and interferences for measuring glyoxal and methyl glyoxal are given in Pang et al. (2014).

With methyl glyoxal detection, moisture within an air sample can lead to an interference from water cluster adducts. As sample humidity increases, the background signal from the protonated water cluster (H$_2$O)$_4\cdot$H$^+$ increases, elevating background noise on the $m/z = 73$ mass channel and changing the methyl glyoxal limit of detection. With calibration of the instrument response to changing chamber temperature and humidity it is possible to correct for interference from isobaric water clusters. In this study the $m/z = 73$ Da signal for methyl glyoxal-H$^+$ was used to analyse the concentration of methyl glyoxal. The linear range for methyl glyoxal is 1.5–172 ppbv by PTR-ToF-MS measurement with a limit of detection of 1.5_1 ppbv (3σ for 3 min averaging) using dry nitrogen as a carrier. The instrumental error on the methyl glyoxal measurement is $\pm 0.8_6$ ppbv.

2.1.6 University of Wisconsin, Madison laser-induced phosphorescence (Mad-LIP)

The Mad-LIP light source is a pulsed, narrow bandwidth (< 0.00078 nm), doubled Ti:Sapphire laser (Photonix Ind.) that is operated at 3 kHz and 20–70 mW. It is further capable of rapid and reproducible wavelength tuning on the scale of the vibro-rotational absorption spectral features of glyoxal (~ 0.06 nm, 440.138 and 440.104 nm on and off band center wavelengths) that are exploited for its detection as discussed below. The emitted laser light is then directed through a White-type multi-pass cell, typically operated at 32 passes and 100 Torr. Gas is drawn through the cell via a scroll pump (Edwards) orthogonal to the laser beam path. During ambient operation, the gas flow is nominally ~ 20 standard L min^{-1} that was reduced to ~ 3 standard L min^{-1} for the first half of the comparison to be increased to ~ 13 standard L min^{-1} in the later half for operational reasons. As a result of the initial flow being very different from standard field operating conditions, operational problems occurred during calibrations. These were accounted for after the fact but resulted in extensive instrument maintenance, which resulted in variability

of the alignment of the multi-pass cell not observed during standard field operation. The variability of the alignment is reflected in variability of the calibration factors as changes in alignment effect (1) throughput how much light is scattered by the mirrors or absorbed/scattered by the baffles as opposed to exciting glyoxal, and (2) the position of the beams relative to the focal point of the PMT (photo-multiplier tube) assembly (changing the collection efficiency of the detector relative to the excitation light and is not well captured by the normalization to laser power). The detection axis is orthogonal to both the laser and gas axis. The detector for phosphorescence photons is a single photon counting PMT guarded by a 520 ± 20 nm bandpass filter (Barr Associates). The interior of the detection cell was optically baffled to reduce laser and ambient light scattering and/or reflecting into the detector.

The Mad-LIP instrument detects both glyoxal and methyl glyoxal by phosphorescence. This is initiated in either analyte by absorption of the laser light, after which, they relax by emission of a phosphorescent photon or are quenched collisionally. As a result, the amount of phosphorescent photons emitted by either is linearly proportional to the optical cross section, which is a function of wavelength described by their respective absorption spectra, the intensity of light, and analyte number density. Both glyoxal and methyl glyoxal signals are normalized by laser power to account for its variation. The photons between 2.5 and 37.5 µs after each laser pulse during a period of integration are summed and recorded as the signal during this time. Due to this gate and delayed photon counting, combined with a 520 ± 5 nm bandpass filter, the effect from laser scatter and fluorescent photons are diminished, minimizing the signal background, and, in particular eliminating any detection of NO$_2$ fluorescence.

The PMT signal (S_{total}) is a linear combination of several components: dark counts (S_{dark}), light scatter (S_{scatter}), glyoxal phosphorescence (S_{gly}) and methyl glyoxal phosphorescence (S_{mgly}). The glyoxal mixing ratio (Glyoxal$_{\text{mr}}$) is proportional to the difference in S_{total} at two different wavelengths: one at high glyoxal absorbance ($\lambda_1 = 440.138$ nm) and another at low glyoxal absorbance ($\lambda_2 = 440.104$ nm, Fig. S1 in the Supplement and Eq. 3). S_{total} is expressed in Eq. (2), followed by the calculation of Glyoxal$_{\text{mr}}$ in Eq. (3).

$$S(\lambda)_{\text{total}} = S_{\text{dark}} + S_{\text{scatter}} + S(\lambda)_{\text{gly}} + S_{\text{mgly}}, \tag{2}$$

$$\begin{aligned} \text{Glyoxal}_{\text{mr}} &= [S(\lambda_1)_{\text{total}} - S(\lambda_2)_{\text{total}}] \cdot \eta_{\text{gly}} \\ &= \big[[S_{\text{dark}} + S_{\text{scatter}} + S(\lambda_1)_{\text{gly}} + S_{\text{mgly}}] \\ &\quad - [S_{\text{dark}} + S_{\text{scatter}} + S(\lambda_2)_{\text{gly}} + S_{\text{mgly}}]\big] \cdot \eta_{\text{gly}} \\ &= [S(\lambda_1)_{\text{gly}} - S(\lambda_2)_{\text{gly}}] \cdot \eta_{\text{gly}}, \end{aligned} \tag{3}$$

where η_{gly} is the calibration factor relating glyoxal mixing ratio to the net glyoxal signal ($S(\lambda_1)_{\text{gly}} - S(\lambda_2)_{\text{gly}}$). The intensity of dark counts is a characteristic of the PMT, and light scatter as well as methyl glyoxal absorption are the

same at λ_1 and λ_2. The calibration factor is determined by introducing a known amount of glyoxal by diluting a calibration standard quantified by CRDS and introducing it into the White-type multi-pass cell. See the CRDS system description as well as theory of operation later in this section. A very high degree of selectivity for glyoxal is achieved using this wavelength dithering approach coupled with monitoring only phosphorescent emission. Only molecules that absorb at ~ 440 nm, phosphoresce at ~ 520 nm, and have similar absorption spectra to glyoxal would be able to interfere. To the authors' knowledge, the Mad-LIP instrument has not observed any interferences with glyoxal detection.

Because S_{gly} is proportional to the glyoxal optical cross section at $\lambda_1 (1.02 \times 10^{-18}$ cm^2 molecule^{-1}), and the net glyoxal signal is proportional to the difference in optical cross section at λ_1 and λ_2 (3.42×10^{-19} cm^2 molecule^{-1}, Volkamer et al., 2005b), the contribution of glyoxal at λ_1 is calculated in Eq. (4). This is then substituted into Eq. (2), and is solved for S_{mgly}, and related to the mixing ratio of methyl glyoxal (methyl glyoxal$_{\text{mr}}$) by a calibration factor (η_{mgly}).

$$S(\lambda_1)_{\text{gly}} = \left(\frac{\sigma(\lambda_1)_{\text{gly}}}{\sigma(\lambda_1)_{\text{gly}} - \sigma(\lambda_2)_{\text{gly}}} \right) \cdot \big(S(\lambda_1)_{\text{gly}} - S(\lambda_2)_{\text{gly}}\big) \tag{4}$$

$$\begin{aligned} \text{Methylglyoxal}_{\text{mr}} &= [S(\lambda)_{\text{total}} - S_{\text{dark}} - S_{\text{scatter}} \\ &\quad - \left(\frac{\sigma(\lambda_1)_{\text{gly}}}{\sigma(\lambda_1)_{\text{gly}} - \sigma(\lambda_2)_{\text{gly}}} \right) \cdot (S(\lambda_1)_{\text{gly}} - S(\lambda_2)_{\text{gly}})\big] \cdot \eta_{\text{mgly}} \end{aligned} \tag{5}$$

The calibration factor for methyl glyoxal is determined in an analogous way as glyoxal via CRDS. Due to the lack of structured absorption of methyl glyoxal (Meller et al., 1991; also see Fig. S1 in the Supplement), Mad-LIP does not possess as high of selectivity for methyl glyoxal as for glyoxal. Additionally, the maximum absorption of methyl glyoxal is about 3 times lower than the maximum of glyoxal absorption at λ_1. Furthermore, the quantum yield of phosphorescence for methyl glyoxal is lower than that of glyoxal. Due to these three reasons, methyl glyoxal has a much higher limit of detection and is susceptible to interferences due to small concentrations of glyoxal.

Instrumental calibrations were performed using cavity ring-down spectroscopy (CRDS), an absolute quantification method in that it relies only on well-documented absorption cross sections. Further details about the theory of this method are described elsewhere (O'Keefe and Deacon, 1988).

A cavity 62 cm long and 0.635 cm in diameter was formed between two parallel, highly reflective mirrors with a radius of curvature of 1 m (99.995 % reflectance, Los Gatos Research Inc.). The bulk of the cavity was encased in a 3/8 inch OD (outside diameter), 1/4 inch ID (inside diameter) PTFE tube. Halfway along the cavity, a PTFE tee was used as an inlet for the calibrant gas. On each end of the cavity, the

mirror mounts were coupled via metal bellows to a Teflon PTFE tee which coupled the cell to exhaust ports for the cell. The dead volumes between the exhaust ports and the mirrors were flushed with zero air through a 200 standard $cm^3 min^{-1}$ flow controller (1779A, MKS Instruments) to prevent optics fouling as well as bias. This purging did not allow any sample gas to mix beyond the exhaust ports, fixing the physical absorber path length to 42 cm. This cell design is based on to the NOAA NO_3 ring-down cell design (Dubé et al., 2006; Osthoff et al., 2006). The entire cavity length between (and including) the exhaust tee fittings was enclosed in a 1.5×1.5 inch block of aluminum which was maintained at a constant temperature (35 °C) to discourage analyte deposition inside the cavity.

A 10 standard $cm^3 min^{-1}$ flow controller (MKS Instruments) supplied calibrant gas that was then diluted by zero air. The zero air was delivered by a 200 standard $cm^3 min^{-1}$ flow controller (MKS Instruments) at a rate which made up the remainder to a total flow of 100 standard $cm^3 min^{-1}$ of diluted calibrant. The purge was held at 100 standard $cm^3 min^{-1}$ using a 200 standard $cm^3 min^{-1}$ flow controller (MKS Instruments). To maintain a constant cell pressure and therefore achieve a stable baseline, both the purge and the diluted calibrant flows were held constant. Laser pulses were introduced into the cavity through one of the high-reflectivity mirrors. A beamsplitter placed between the light source and the White-type multipass cell supplied light to the CRDS cell. With each reflection of a laser pulse, a small quantity of light escaped through the mirrors. On the opposite side of this cavity, a PMT (Hamamatsu), guarded by a 440 nm bandpass filter, detected this escaped light. Loss of photons within the cavity is a first-order process; thus, the light leaking from the cavity has the characteristics of an exponential decay. The number density of a chemical absorber (molecules cm^{-3}) can be determined by relating two determined lifetimes, those determined with and without the presence of the absorber, by the following equation:

$$N_d = \left(\frac{1-R}{\sigma l_a} \right) \left(\frac{\tau_0 - \tau}{\tau} \right),\qquad(6)$$

where N_d is the number density of the absorber, R is mirror reflectivity, σ is the absorption cross section (either Volkamer et al., 2005b, or Meller et al., 1991) for glyoxal and methyl glyoxal, respectively), l_a is the path length of the absorber, τ and τ_o are the lifetimes with and without the absorber, respectively (Zalicki and Zare, 1995).

2.1.7 CEAM white-cell DOAS (W-DOAS)

A Differential Optical Absorption Spectroscopy device using a white multi-reflection cell (W-DOAS) of 8 m base path-length is deployed at EUPHORE. The optical system employed a Xenon high pressure short-arc lamp (XBO-550W) as the light source, coupled to a telescope that collimates the light into a narrow beam and sends it into the chamber. The

multi-reflection cell used during these experiments consisted of a set of prisms and mirrors dielectrically coated, allowing an optical path of 1154 m with reflection of the beam in the range 389–469 nm, for the detection of glyoxal, methyl glyoxal and NO_2. Two laser diodes and web-cameras were used to adjust the path-length of the system. The beam is finally driven outside of the chamber where it is focused by a telescope onto the entrance slit of a spectrograph equipped photodiode array detector. A detailed description can be found in Becker (1996).

The system collected spectra every 80–110 s by co-addition of 100 samples. A blank spectrum taken at the beginning of each day in the clean chamber was used as background $I_0(\lambda)$. Also, during the experiment, the stray-light was corrected by subtracting a spectrum recorded by introducing an edge filter in the light beam. The resolution was set to 0.35 nm FWHM. The analysis of the data was performed using a fitting routine (Rodenas, 2008) adapted to process DOAS data; this fitting routine was successfully tested in previous intercomparison exercises (Rodenas, 2008). The same literature cross sections for glyoxal, methyl glyoxal and NO_2 as the other instruments were used.

2.1.8 CEAM Fourier transform infrared spectrometer (CEAM FTIR)

The EUPHORE chamber is equipped with a Fourier Transform Infrared system (FTIR). The spectrometer (NICOLET 550, MCT/B-detector) is coupled to a white-type multi-reflection cell installed into the chamber for the detection of gaseous reactants and products in the IR spectral range (400–4000 cm^{-1}). The gold-coated mirrors of the cell allow a total path length of 616 m (8.3 m base path). With FTIR, it is possible to calculate the concentration of a wide range of compounds and reaction products using absorption reference spectra previously collected and the corresponding calibration thereof. A detailed description of the instrument is given in Becker (1996).

The spectra were derived from the co-addition of 280 scans, collected over a 5 min period, with a resolution of 1 cm^{-1}. During the experimental campaign, concentration profiles of glyoxal and methyl glyoxal were determined using improved analysis software developed at CEAM (Rodenas, 2008) adapted to analyze infrared spectra, and applied to the region of 2700–2900 cm^{-1}. This program is based on a classical least squares fitting which also removes the spectral interfering broadband (formed due to the presence of aerosols, equipment instabilities or unknown broadband products) by including a curve that models and subtracts it locally. The software has been tested and used in previous works (Muñoz et al., 2011, 2012).

Reference spectra were previously collected with the instrument, and calibrated with the references used by the W-DOAS system (Sect. 2.1). Water, formaldehyde, methanol and other compounds show absorption bands in the same

spectral region as glyoxal and methyl glyoxal. Together with these compounds, the instrument was used to report the evolution of most of the reactants and products forming the complex mixture in the experiments preformed. These compounds were present in the samples to a greater or lesser degree depending on the experiment carried out. The fitting was done using both the aldehydic C-H band and the region 770–1140 cm^{-1}. The list of compounds analyzed includes ozone, isoprene, nitric acid, o-xylene, and formic acid. SF$_6$ was also monitored by FTIR to quantify the dilution range of the chamber.

2.1.9 CEAM Solid-phase microextraction (SPME)

Solid-phase microextraction (SPME) methodology was used to determine glyoxal and methyl glyoxal through PFBHA on-fiber derivatization. A detailed description of the methodology used at the EUPHORE chambers can be found in the literature (Gómez Alvarez et al., 2007; Alvarez and Valcárcel, 2009). Briefly, the SPME device used in this work consisted of a holder assembly with 65 μm fibers coated with Polydimethylsiloxane/Divinylbenzene (PDMS/DVB), from Supelco, Bellefonte, PA (USA). These fibers were conditioned following the manufacturer's recommendations for at least 0.5 h at 250 °C to eliminate any impurities. Fibers were loaded with PFBHA derivatization reagent, for 2 min, through the headspace of a 4 mL opaque amber vial containing a 17 mg mL^{-1} PFBHA water solution.

Exposing the fiber to the air of the chamber was achieved by means of an aluminum adapter located in one of the flanges in the chamber floor. In the exposed position, fibers extend into the chamber by a few millimeters.

Samples were taken for several minutes and were subsequently analyzed by GC-FID by injecting the fiber directly into the GC injector. Sampling time ranged depending on the dicarbonyl concentrations. Whenever possible, identification of the peaks was also cross-checked using GC-MS. The chromatographic conditions were as follows: a 6890 HP gas chromatograph was used, coupled to a flame ionization detector (FID), equipped with a HP5-MS capillary column (30 m × 0.25 mm ID × 0.25 μm) and an inlet liner with a narrow internal diameter 0.75 mm ID pre-drilled Thermogreen LB-2 septa for SPME were used. The chromatograph was programmed at 80 °C for 2 min, then ramped at a rate of 20–280 °C and held at 280 °C for 3 min. The injection port was held at 270 °C and detector at 300 °C. Samples were injected in splitless mode, using on column constant helium flow of 1 mL min^{-1}.

2.2 NCAR Chamber and experimental conditions

A set of chamber experiments was carried out using the temperature-controlled simulation chamber at the National Center for Atmospheric Chemistry (NCAR) to study the temperature dependence of glyoxal and methyl glyoxal calibra-tions (January–March 2011; March–April 2012). The chamber consists of a stainless steel cylinder ($\sim$ 47 L) connected to a Fourier transform infrared spectrometer, as previously described in the literature (Shetter et al., 1987; Orlando and Tyndall, 2002; see Fig. 1a). The chamber was chilled by circulating ethanol to cool the chamber to 260 K or heated (320 K) by circulating water. See Table 1 for the list of experiments. Reactant gases (typical starting concentrations $3-7 \times 10^{14}$ molecules cm^{-3}; 11–26 ppm) were injected from a calibrated bulb into the chamber via a gas line as described previously (Orlando and Tyndall, 2002). The chamber was pressurized above ambient pressure and a small amount of gas (20–30 standard cm^3 min^{-1}) was leaked from the chamber through one port and divided and diluted (a factor of 100 dilution for CE-DOAS and a factor of 50 dilution for PTR-ToF-MS) before going to the sampling instruments. Reaction chemistry was initiated by adding light from a filtered Xe arc lamp or by injection of O$_3$ in presence of an alkene.

In the NCAR chamber glyoxal was produced by the oxidation of acetylene (C$_2$H$_2$, ethyne) by either Cl or OH radicals. Starting gases (reactants, oxygen) were injected into the chamber and the entire volume was diluted with nitrogen to 800 Torr. Methyl glyoxal was produced in a similar fashion from the oxidation of hydroxyacetone (CH$_3$C(O)CH$_2$OH, HACET) by Cl atoms.

2.3 EUPHORE chamber and experimental conditions

The EUPHORE facility consists of two 200 m^3 hemispherical Teflon enclosures with retractable roofs to allow for ambient illumination of the chambers for radical production. Figure 1b shows the layout of the Chamber A of the EUPHORE facility during the experimental campaign including the locations of the various instrument sampling ports, gas injection and circulation. Samples were injected into the chamber via an air stream added through center ports and mixed in the chamber by two fans. The chamber was operated at ambient temperature and approximate pressure using scrubbed air and homogeneously mixed using two horizontally and vertically mounted fans (see Fig. 1b). Chamber dilution is followed throughout each experiment using an inert SF$_6$ tracer (Becker, 1996; Muñoz et al., 2014).

At the EUPHORE facility 10 experiments were carried out from 24 June–6 July 2011. These experiments consisted of the injection of pure glyoxal (experiments E1 and E8) or methyl glyoxal (E2) which were subsequently diluted in steps, as well as the simultaneous in situ production of these compounds from the (photo) oxidation of precursors (isoprene, experiments E4, E7, and o-xylene, E3). Additionally, the instruments were tested for interferences in the chamber from other species, such as NO$_2$ (experiments E9 and E10), biacetyl (butane-2,3-dione, CH$_3$C(O)C(O)CH$_3$; E3), aerosol (E3) with filtered/unfiltered optical instruments and O$_3$ (E5, possible production of glyoxal from O$_3$ reacting with Teflon).

Table 3. Correlation data for instruments vs. CE-DOAS for individual experiments.

Exp #	Species	Instrument	# pts	Slope	Intercept (ppbv)	R^2	Avg t (min)
			Pure compound experiments				
NCAR[a]	GLY	FT-IR	19	1.02(2)	$5(4) \times 10^{11}$[b]	0.996	4
NCAR[a]	MGLY	FT-IR	25	1.00(1)	$1.2(7) \times 10^{12}$[b]	0.996	4
N7	MGLY	PTR-ToF-MS	5	0.95(3)	$8.5(10) \times 10^{12}$[b]	0.997	4
NCAR[a]	NO$_2$	FT-IR	80	1.06(2)	$-2(4) \times 10^{12}$[b]	0.98	4
E1	GLY	BBCEAS	492	0.970(2)	−0.005(2)	0.9997	1
E1	GLY	Mad-LIP	338	0.82(1)	−0.003(1)	0.9998	1
E1	GLY	W-DOAS	284	0.917(3)	−0.06(1)	0.9998	1.5
E1	GLY	FT-IR	13	0.98(3)	0.1(7)	0.999	10
E1	GLY	SPME	15	0.95(10)	−0.01(1)	0.996	5
E1	GLY	CE-DOASb[e]	492	0.98(1)	0.17(10)	0.998	1
E8a	GLY	BBCEAS	546	0.967(5)	−0.012(2)	0.9998	1
E8a	GLY	Mad-LIP	528	1.11(2)	−0.002(3)	0.998	1
E8a	GLY	W-DOAS	239	0.916(7)	−0.07(2)	0.998	1.5
E8a	GLY	FT-IR[c]	53[c]	0.99(2)[c]	−0.2(1)[c]	0.992	10
E8a	GLY	SPME	14	0.85(8)	0.00(1)	0.998	10
E8a low[d]	GLY	BBCEAS	316	1.009(9)	−0.021(3)	0.9994	1
E8a low[d]	GLY	Mad-LIP	239	1.17(2)	−0.006(4)	0.997	1
E8a low[d]	GLY	W-DOAS	144	0.68(5)	−0.03(2)	0.87	1.5
E2	MGLY	BBCEAS	503	1.010(3)	0.36(2)	0.9987	1
E2	MGLY	Mad-LIP	503	1.43(2)	−0.08(3)	0.997	1
E2	MGLY	FT-IR	55[c]	1.174(13)[c]	0.65(13)[c]	0.996	10
E2	MGLY	PTR-ToF-MS	375	1.231(5)	−1.05(2)	0.96	10
E2	MGLY	W-DOAS	228	0.97(3)	−0.2	0.96	1.5
			Mixed compound experiments				
E3	GLY	BBCEAS	348	0.988(3)	−0.012(2)	0.999	1
E3	GLY	Mad-LIP	211	0.83(1)	−0.034(2)	0.998	1
E3	GLY	W-DOAS	240	0.88(2)	−0.22(8)	0.97	1.5
E3	GLY	FT-IR[c]	58[c]	1.5(1)[c]	0.95(10)[c]	0.88[c]	10
E3	GLY	SPME	10	1.1(2)	0.08(2)	0.98	5
E3	MGLY	BBCEAS	316	0.92(2)	0.17(2)	0.97	1
E3	MGLY	Mad-LIP	240	1.66(3)	0.13(4)	0.95	1
E3	MGLY	FT-IR	58	1.3(1)	0.3(1)	0.99	10
E3	MGLY	SPME	10	0.86(13)	0.5(1)	0.65	5
E3	NO$_2$	BBCEAS	345	1.0087(8)	0.046(3)	0.998	1
E3	NO$_2$	W-DOAS	240	0.95(1)	0.14(2)	0.994	1.5
E5	GLY	BBCEAS	567	1.023(4)	−0.053(2)	0.99995	1
E5	GLY	Mad-LIP	241	f	f	f	1
E5	GLY	FT-IR	79	1.07(1)	−0.4(1)	0.998	10
E6	NO$_2$	BBCEAS	505	0.98(2)	0.02(2)	0.995	1
E6	GLY	BBCEAS	505	0.95(1)	−0.19(4)	0.987	1
E6	GLY	Mad-LIP	308	1.09(2)	−0.005(5)	0.97	1.5
E6	GLY	SPME	14	1.5(2)	0.04(5)	0.79	5
E6	MGLY	BBCEAS	505	0.68(3)	0.17(5)	0.68	1
E6	MGLY	Mad-LIP	308	1.90(6)	−0.1(1)	0.58	1.5
E6	MGLY	SPME	14	0.7(2)	0.2(2)	0.69	5
E7	NO$_2$	BBCEAS	553	0.985(4)	−0.27(1)	0.999	1
E7	GLY	BBCEAS	553	0.927(3)	−0.034(3)	0.999	1
E7	GLY	Mad-LIP	326	1.47(2)	−0.033(6)	0.993	1.5
E7	GLY	FT-IR[c]	111[c]	2.5(1)[c]	−0.2(1)[c]	0.93[c]	10
E7	GLY	SPME	10	1.3(1)	0.04(4)	0.95	5
E7	MGLY	BBCEAS	553	0.92(1)	−0.20(4)	0.987	1
E7	MGLY	Mad-LIP	326	2.21(4)	0.6(1)	0.98	1.5
E7	MGLY	FT-IR[c]	111[c]	0.68(4)[c]	−0.6(2)[c]	0.84[c]	10
E7	MGLY	SPME	14	0.7(1)	1.3(5)	0.65	5

Number in parenthesis is the 1-σ uncertainty of the last digit of the number; [a] NCAR experiment data are pooled over experiments listed in Table 2 (for GLY and MGLY) or for all oxidation experiments in 2011 and 2012 (30+ experiments at three different chamber temperatures); [b] intercepts in molecules cm^{-3} due to the constant volume of the chamber and the changing pressure and temperature over the course of more than 30 different experiments (as described in note a); [c] experiment near detection limit; [d] only concentrations below 2 ppbv fitted for instruments with applicable detection limits; [e] results from fit of the weak glyoxal bands (see Sect. 2.1.3); [f] result is non-linear, Fig. S7.
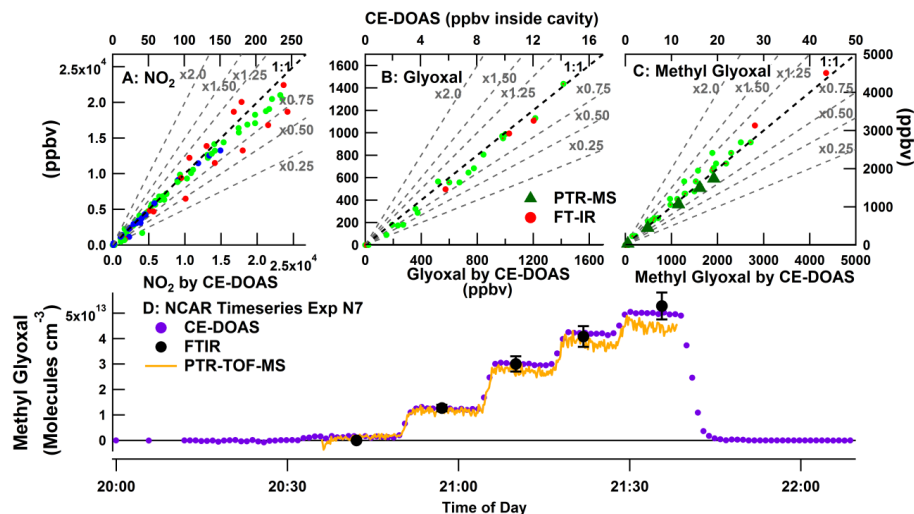
Figure 2. Correlation of FT-IR and PTR-ToF-MS relative to CE-DOAS for experiments N1–N9 at NCAR (NO$_2$ includes additional experiments, see text). Data from individual experiments have been pooled at different temperatures. **(a–c)** FT-IR (dots), PTR-ToF-MS (triangles), three temperatures (blue – 260 K, green – 293 K, red – 330 K). **(d)** Time series for experiment N7 to produce methyl glyoxal. For display on these graphs, units in **(a–c)** (molecules cm^{-3}) have been converted to volume mixing ratios using a single chamber temperature and pressure (295 K, 800 Torr) representing the typical conditions at the start of room temperature experiments.

The full list of experiments along with experiment objectives are listed in Table 2.

The photo-oxidation experiments (*o*-xylene and isoprene oxidation) are rapidly evolving, complex chemical systems and hence there is potential for interferences from a wide range of α-dicarbonyls (glyoxal, methyl glyoxal and biacetyl) co-products such as unsaturated 1,4-dicarbonyls and furanones (from *o*-xylene) and glycolaldehyde and hydroxyacetone (isoprene). In addition a reasonable amount of SOA is formed in the *o*-xylene experiment.

Glyoxal and methyl glyoxal were prepared as described in the literature: pure glyoxal monomer was prepared from the solid trimer-dihydrate using the methods described in Feierabend et al. (2007) with minor modification. Pure methyl glyoxal monomer was prepared from 40 % aqueous solution after one night pumping to eliminate most of the water using the method describe in Talukdar et al. (2011) with minor modifications. Cold fingers containing pure samples of un-polymerized glyoxal or methyl glyoxal were temporarily kept at liquid nitrogen temperatures prior to experimental use. Glyoxal and methyl glyoxal were introduced into the chamber by passing a small flow of nitrogen through a gently warmed cold-trap.

3 Results

The data from all instruments was analyzed by the individual groups and then correlations were calculated with respect to CE-DOAS for the data from NCAR and between each instrument pair for the EUPHORE experiments. In order to account for differences in time resolution between different in-

struments the data points were averaged to the longest time interval of any given instrument pair (see Table 3 for time resolution of the instruments), and data points a few minutes after injection periods were removed to avoid any effects due to the instruments sampling unmixed gas from the chamber. Correlations were calculated in IGOR Pro (WaveMetrics) using the optimal distance regression (ODR) function, to account for uncertainty along both axes ($y - y$ regression).

3.1 NCAR

The CE-DOAS, PTR-ToF-MS and FTIR instruments at NCAR used independent sources of calibration, and provide an opportunity to assess our understanding of the underlying absorption cross-section data at UV-visible and IR wavelengths, as well as compare these cross sections with ion–molecule rate constants (in the case of methyl glyoxal). No signal was observed for glyoxal in the PTR-ToF-MS (up to 32 ppbv glyoxal was supplied to the PTR inlet after dilution). PTR-ToF-MS data for methyl glyoxal was corrected for interference of the isobaric water cluster peak that gave an initial background signal at the methyl glyoxal peak (see Fig. S2). Correlation plots for glyoxal and methyl glyoxal did not show significant intercepts and were independent of temperature (295 and 320 K). Correlations for NO$_2$ (for CE-DOAS and FTIR only) agreed within ±5 % ($R^2 = 0.99$) and were independent of temperature (260, 295 and 320 K) but had lower R^2 values (0.95) due to non-linearity in the FTIR when high concentrations ($> 4 \times 10^{14}$ molecules cm^{-3}) were included. The results of these correlations are shown in Table 3, and a time series of one methyl glyoxal experiment is shown in Fig. 2. Figure 2a–c include data from 20 different
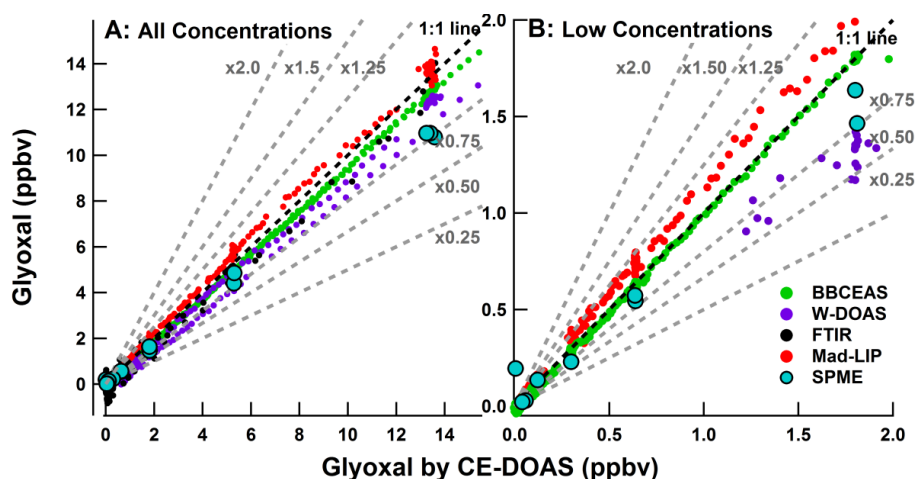
Figure 3. Correlations for the glyoxal comparison experiment E8a (see Fig. S8a for a time series of these points). **(a)** Full concentration range; **(b)** concentrations below 2 ppbv. Data are only shown from instruments where the maximum concentration exceeds the LOQ (see Sect. 4.2).

experiments for NO$_2$, and 5 experiments each for glyoxal and methyl glyoxal; averages are shown in Fig. 2.

3.2 EUPHORE

3.2.1 Glyoxal intercomparison

Experiments E1 and E8a consisted of the injection of pure glyoxal into the chamber followed by stepped dilution. Correlations of data segregated between high (0–15 ppbv) and low (0–2 ppbv) mixing ratio data are shown in Fig. 3. It should be noted that the W-DOAS instrument is affected by the distortion of the light beam during the flushing of the chamber (the air input of the flushing is in the center of the chamber and intersects the W-DOAS light path). Table 3 compares individual instruments to CE-DOAS; correlation matrices that compare each instrument pair-wise to each other instrument for experiments E1 and E8a can be found in Tables S1–S2 in the Supplement. The slopes varied between 0.76 and 1.09 between all instruments and both experiments. Mad-LIP defines the highest and lowest slopes observed, reflecting $\sim 33\%$ difference in separate calibrations between both experiments as well as different operating conditions (see Sect. 2.1.6). All other instruments agreed within 15%.

Experiment E9 investigated the possible interference of a large amount of NO$_2$ on detection of glyoxal for instruments using visible (430–490 nm) light spectroscopy and found no scalable bias due to NO$_2$. In this experiment the Mad-LIP was used as the glyoxal reference to evaluate effects of NO$_2$ with the UV-visible absorption techniques as previous work by Huisman et al. (2008) had shown Mad-LIP measurements of glyoxal to be insensitive to NO$_2$ interferences, tested up to 1 ppmv. Figure 4 shows the time series of glyoxal and NO$_2$ concentrations for E9. The initial glyoxal amount (0.6 ppbv) was diluted and left to stabilize around 0.3 ppbv in absence of

NO$_2$, followed by stepped NO$_2$ additions up to ~ 180 ppbv. SF$_6$ was added and measured by FTIR as a tracer for dilution. The SF$_6$ signal in Fig. 4 has been scaled to the initial glyoxal and shows that the theoretical decay according to dilution of the glyoxal glyoxal signal is in good agreement with the Mad-LIP glyoxal data. Note that the error bars increase at high NO$_2$, more for CE-DOAS than for BBCEAS due to larger light losses at the longer absorption path in CE-DOAS. Deviations in glyoxal however were small for all instruments; they are marginally significant for BBCEAS and insignificant for CE-DOAS during periods when MAD-LIP data is available (see Fig. 5). Deviations in the SPME concentrations were large but appear to be unconnected to the high NO$_2$ levels in the chamber. For both CE-DOAS and BBCEAS (Figs. 4 and 5) we do not find significant bias; i.e., an upper-limit change in glyoxal due to NO$_2$ is derived as ± 200 pptv glyoxal in the presence of 200 ppbv NO$_2$ (or bias of 1 pptv glyoxal/1 ppbv NO$_2$).

3.2.2 Methyl glyoxal intercomparison

Experiment E2 compared methyl glyoxal measurements in a pure compound system. Approximately 25 ppbv of methyl glyoxal was injected into the chamber, and diluted in 6 discrete steps to less than 1 ppbv. Figure 6 shows correlation plots of data segregated into high and low (< 3 ppbv) concentrations, and the regression lines (see Table 3). The slopes varied between 0.97 and 1.40, with generally larger differences in slopes between instruments than for glyoxal. Mad-LIP showed the highest slope, while W-DOAS had the lowest slope. Experiment E10 tested the interference of NO$_2$ on methyl glyoxal, as previously described for glyoxal (Sect. 3.2.1). The initial level of methyl glyoxal was 5.3 ppbv (Fig. S3), and the SF$_6$ dilution signal was used as the dilution reference. For FTIR the concentrations were high enough
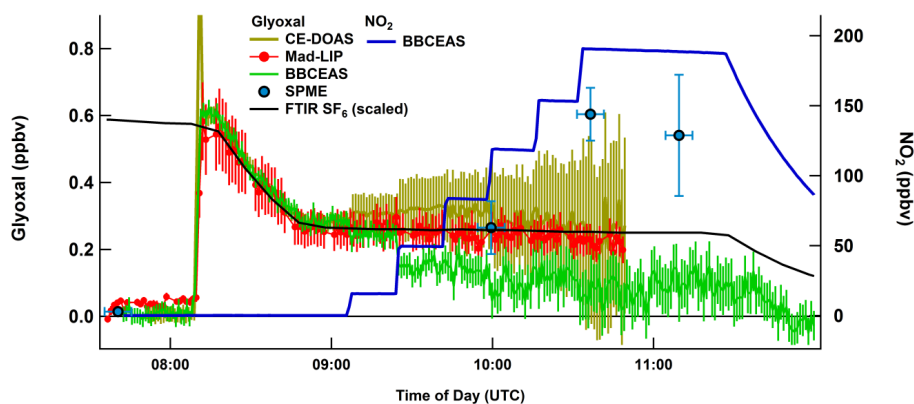
Figure 4. Sensitivity of glyoxal to high levels of NO$_2$ (experiment E9). Chamber dilution has been scaled relative to concentrations at 08:15 UTC from the decay of the SF$_6$ tracer. See text for details. The error bars are the sum of the statistical uncertainty for retrieving the absorber's concentration from the spectral structure and the systematic uncertainties in determining the cavity mirrors' reflectivity, the cavity's length factor and the uncertainties reported on the literature absorption cross sections used to fit the BBCEAS/CE-DOAS spectra (see Sect. 2.1.4 and in the Supplement).
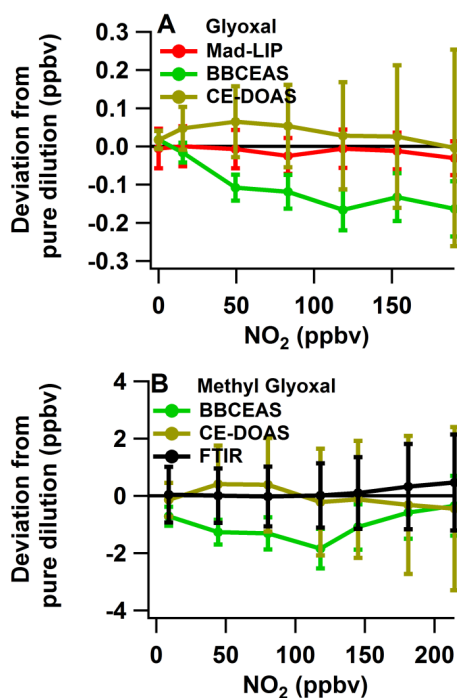
Figure 5. Deviations from pure dilution in the chamber for experiments 9 and 10 relative to NO$_2$ in the chamber. No clear trend is apparent over the full range of NO$_2$ investigated.

to obtain good signal, and the methyl glyoxal and NO$_2$ absorption are well separated at IR wavelengths. No significant deviations in methyl glyoxal were observed in CE-DOAS and BBCEAS, and excellent agreement is observed even in excess of 200 ppbv NO$_2$ (see Fig. 5b). In the presence of 200 ppbv we found a maximum bias of ±1 ppbv on a sam-

ple of 5.3 ppbv methyl glyoxal (or a bias of 5 pptv methyl glyoxal/1 ppbv NO$_2$; see Figs. 5 and S3).

3.2.3 Dry photochemical smog systems

Experiment E3 investigated *o*-xylene photo-oxidation by OH radicals in the presence of NO$_x$ (added as HONO), as a source for highly variable concentrations of glyoxal, methyl glyoxal, biacetyl and NO$_2$. Figure 7 illustrates the time series and correlation plots. Table 3 gives the results of regression fits (correlation plots include data from before and after HONO addition and chamber opening). The slopes varied between 0.83–1.1 (glyoxal), 0.86–1.7 (methyl glyoxal), and 0.95–1.01 (NO$_2$), and most instruments agreed within 12, 30, and 5 %, respectively. These differences were similar or slightly larger than those observed in the pure compound experiments (Sects. 3.2.1, and 3.2.2.). Notably, differences of up to 8 % between BBCEAS and CE-DOAS for methyl glyoxal are observed despite excellent agreement (better than 1 %) for both glyoxal and NO$_2$. While Mad-LIP data show excellent correlation ($R^2 > 0.95$ for both α-dicarbonyls, Table 3) they also mark the largest (1.66 methyl glyoxal) and smallest (0.83 glyoxal) slopes for both α-dicarbonyls. Although FTIR performed well for methyl glyoxal, concentrations of glyoxal were close to the detection limit of the FTIR, and the measured concentrations did not scatter around zero as expected (Fig. 7a) most probably due to unknown interfering products formed because the chamber was exposed to light (NO$_2$, ozone and HCHO formation were observed from walls). Hence, FTIR data were only considered for further discussion if values exceeded detection limits by at least a factor of 2 for constructing correlations and 10 for calculation of accuracy (Table 4).

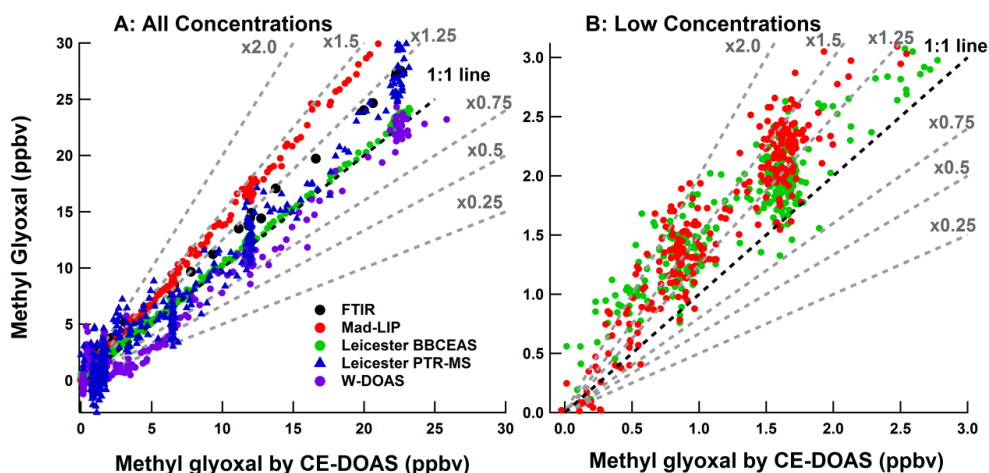In the isoprene/NO$_x$ system (experiment E7, see Fig. S4) results were generally similar. However, the variations in

Figure 6. Correlation plots for methyl glyoxal comparison experiment E2. **(a)** Full range of measured concentrations, while **(b)** shows only concentrations below 3 ppbv. Only data is shown from instruments where the maximum concentration exceeds the LOD (see Sect. 4.2).
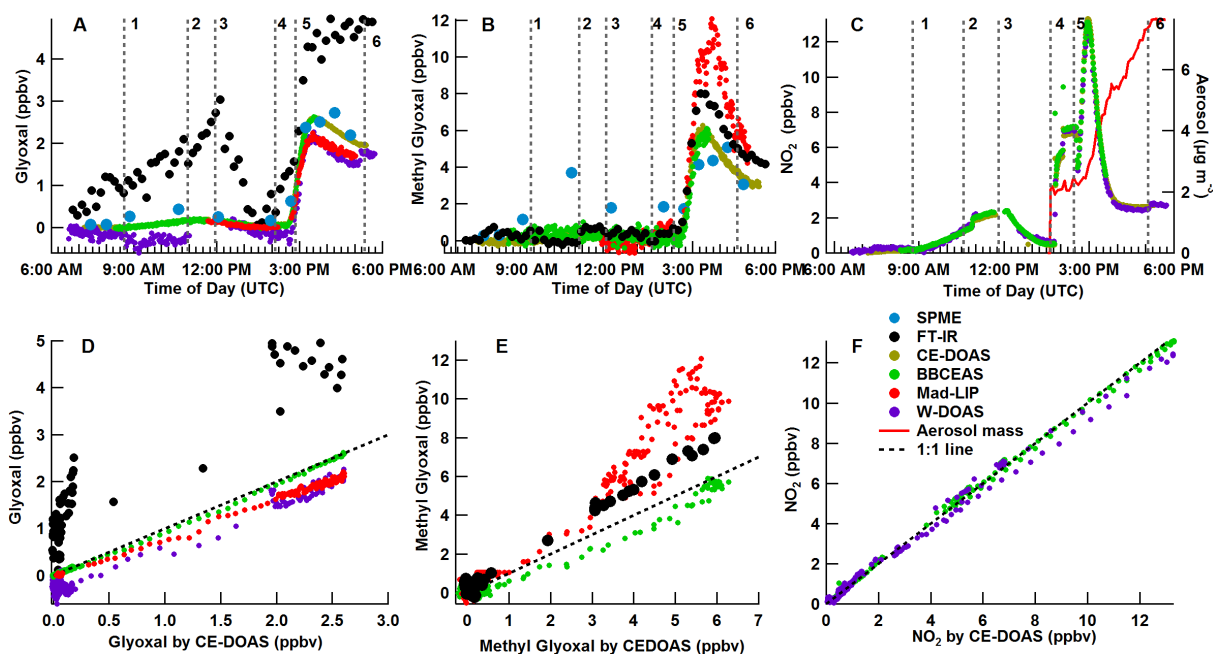

Figure 7. Dry photo-oxidation of *o*-xylene during experiment E3. **(a–c)** show the time traces of glyoxal, methyl glyoxal and NO₂, respectively. **(d–f)** show the correlation plots of the respective compounds. E3 began in the morning with a clean, flushed chamber. The chamber roof was opened (1) while clean and the build-up of NO₂ and other contaminates was observed and then closed (2) and flushed clean (3). In the afternoon, HONO was added to the chamber (4) and with it some NO₂, then the chamber roof was opened (5) to initiate the photo-chemistry and closed to finish the experiment (6).

slopes were somewhat higher, i.e., 0.94–1.54 (glyoxal), and 0.7–2.2 (methyl glyoxal), while most instruments agreed within 30 % for both species (see Table 3). Again, Mad-LIP data show excellent correlation ($R^2 > 0.98$) indicating the shape of the Mad-LIP profile agreed with the other instruments, but there were systematic differences in the slopes (up to a factor of 2.2 for methyl glyoxal). This is indicative of the calibration and stability issues present in the Mad-LIP in-

strument during the campaign (see Sect. 2.1.6) as well as the difficulty in differentiating the methyl glyoxal signal from a large glyoxal background.

Experiment E4 consisted of a higher NO$_x$ isoprene oxidation experiment (NO₂ concentrations up to 170 ppbv) and has been excluded from these comparisons for operational reasons. The NO$_x$ control system failed to maintain a stable NO$_x$ concentration in the chamber and a dilution valve failed

Table 4. Detection limits of all instruments at NCAR and EUPHORE.

| Instrument[b] | Precision (ppbv) | | | | | | Accuracy (%) [a] | | Time |
| | GLY | | | MGLY | | | GLY | MGLY | |
	LOD$_r^c$	LOD$_{var}^d$	LOD$_{Eq. (7)}^e$	LOD$_r^c$	LOD$_{var}^d$	LOD$_{Eq. (7)}$			(min)
CE-DOAS	0.015	0.012	0.015	0.15	0.27	0.28	–	–	1
NCAR FT-IR	50	–	–	92	–	–	–	–	4
NCAR PTR-ToF-MS^d	–	–	–	–	1.2	–	–	–	0.167
CE-DOAS	0.015	0.012	0.015	0.21	0.27	0.28	4	10	1
BBCEAS	0.075	0.045	0.053	1.0	0.6	0.7	7	10^f	1
PTR-ToF-MS	–	–	–	0.53	5.3	–	–	–	1
Mad-LIP	0.06	0.038	0.063	1.2	0.9	1.14	48	80^f	1
W-DOAS	0.4	0.3	0.33	6.0	–	–	4	–	1.5
EUPHORE FTIR	2.5	1.1	1.1	2.7	–	–	10	70	10
SPME with GC-FID detection	0.1	–	–	0.15	–	–	50	20	10

[a] Accuracy evaluated as the 95 % CI of the fitted slopes in correlation plots versus CE-DOAS (Sect. 4.2) for experiments where signal-to-noise was at least 10; accuracy of CE-DOAS is estimated in the Supplement; [b] abbreviations given in the text; [c] operator Reported Detection Limits 3σ; [d] LOD based on measured variability at constant signal (LOD = 3σ ppbv, see Sect. 4.2); width of Histograms in Figs. 9 and 10 for EUPHORE experiments, and as the LOD in the instruments for other background data for NCAR experiments; [e] LOD calculated according to Eq. (7), where |background| is equated to the offset from Figs. 9 and 10; [f] omits E6 due to the lack of variability in the MGLY concentration (see Fig. 8c).

in the CE-DOAS system which prevented the retrieval of the data to compare with other instruments (dilution of the chamber flow into the CE-DOAS system was not attempted on any of the other experiments).

3.2.4 Moist ambient air

For experiment E6, ambient air was added to a cleaned chamber, to assess possible interferences from other species. For example, water vapor absorbs light at blue visible wavelengths, and can create problems with the molecular spectroscopy in UV-visible absorption techniques. Further, the transfer of α-dicarbonyls through sampling lines can become complicated in presence of ambient levels of relative humidity. Aerosols can reduce path length with BBCEAS, and other species in ambient air may create further interferences. Figure 8 shows the time series: a clean chamber was exposed to sunlight, and ambient air was added (see Fig. S5 for correlations of BBCEAS and Mad-LIP with respect to CE-DOAS); the chamber's roof was closed and ~ 100 ppbv O$_3$ was added. Some of the accelerated decrease in NO$_2$ during the following hour may indicate formation of NO$_3$ radicals, and subsequent N$_2$O$_5$ hydrolysis on aerosols and chamber walls. The roof was then opened, and after 1.5 h HONO was added in a defined way such that NO$_x$ (NO + NO$_2$) remained constant. Finally, a small amount of isoprene (18 µL, ~ 25 ppbv in the chamber) was injected while NO$_x$ was controlled via the HONO source. The RH varied between 30 and 50 %, and NO$_2$ levels were below 16 ppbv at all times, while concentrations of α-dicarbonyls varied between 0.1 < glyoxal < 1 ppbv, and 50 pptv < methyl glyoxal < 5 ppbv, with average concentrations of 380 pptv glyoxal, and 1.7 ppbv methyl glyoxal. The slopes of correla-

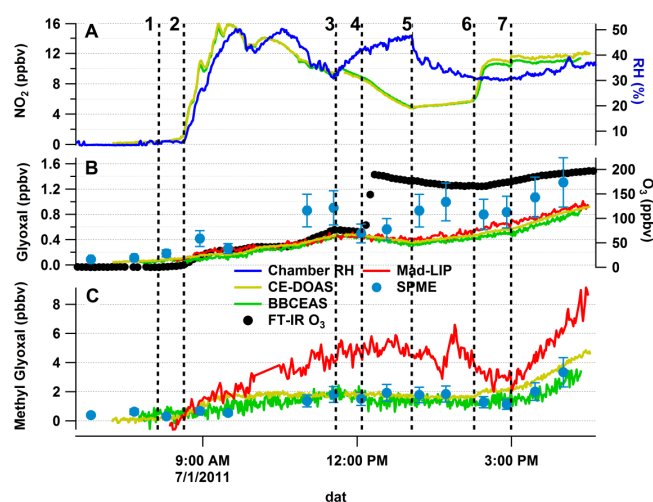**Figure 8.** Ambient air experiment E6. **(a)** shows the NO$_2$ and relative humidity, **(b)** glyoxal and ozone, and **(c)** methyl glyoxal. The chamber operations for the day were as follows: (1) at 8.05 a.m. the chamber roof was opened; (2) the "chamber valve" was open from 8.37–9.30 a.m., allowing ambient air to enter the chamber. After 9.35 a.m. the chamber was closed and is considered to be mixed. (3) The chamber roof was closed at 11.36 a.m., (4) O$_3$ injection (12.09–12.17 p.m.), (5) chamber roof opened 1.03 p.m., (6) start HONO injection for NO$_x$ control (2.15 p.m.), (7) isoprene injection (2.58 p.m.).
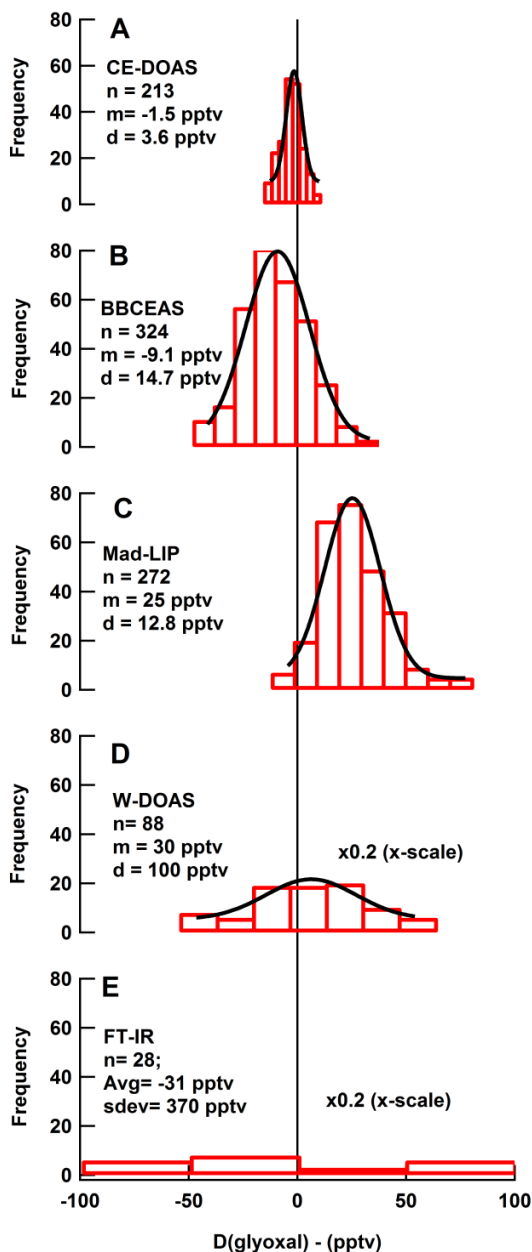
Figure 9. Histograms of glyoxal baseline variability during experiment E8b, 6 July 2011 from 02:00–06:00 UTC. The instruments sampled from a clean chamber. The number of points in the distribution (n), the mean (m) and 1-σ standard deviation (d) are listed on each graph, and experimentally determined limits of detection as quoted in Table 4 were calculated as $\mathrm{LOD}_{\mathrm{exp}} = 3 \times d + |m|$. The time series of the data used to produce the histograms is shown in Fig. S8b and c.

Figure 10. Histograms of methyl glyoxal baseline variability in experiment E8b after 02:00 UTC. The number of points in the distribution (n), the mean (m) in ppbv and 1 standard deviation (d) of the distribution are listed in each panel (**a**: CE-DOAS; **b**: BBCEAS; **c**: Mad-LIP). Histogram distributions are used to calculate experimentally determined limits of detection as $\mathrm{LOD}_{\mathrm{exp}} = 3 \times d + |m|$.

tions (Table 3) varied between 0.95–1.5 (glyoxal), 0.68–1.83 (methyl glyoxal), and 0.995 (NO$_2$) – agreement between most instruments was on the order of 10 % for glyoxal, and 30 % for methyl glyoxal, with extreme slopes showing differences of 50 % in case of SPME-glyoxal, and 83 % in the

case of Mad-LIP methyl glyoxal. Interestingly, CE-DOAS and BBCEAS slopes agreed within 2 % for NO$_2$, 5 % for glyoxal, but differed by 32 % for methyl glyoxal. We note that the range of methyl glyoxal concentrations is fairly limited (correlations are driven by essentially two groups of points one near 0 and the other near 2 ppbv). The cause for this difference is not clear to the authors. A possible partial explanation may exist in the difference in sampling location from the chamber, as CE-DOAS sampled close to the wall of the chamber, and the rise in methyl glyoxal after 3 p.m. that drives the CE-DOAS vs. BBCEAS correlation away from 1 : 1 could be an artefact of wall interaction (and not an instrumental difference). Generally, correlations are slightly more variable in humid air than in dry air, and were found to be slightly lower for methyl glyoxal ($0.58 < R^2 < 0.68$) than

for glyoxal ($0.79 < R^2 < 0.99$). For discussion of the effect of H$_2$O on measurements of low glyoxal and methyl glyoxal concentrations see Sects. 4.5 and 4.6. The effect of ambient levels of NO$_2$ on the glyoxal retrieval from CE-DOAS in E6 is shown in Fig. S6 and discussed more at length in Sect. 4.4.

3.2.5 Interference from O$_3$

Experiment E5 tested the interference of O$_3$ directly via spectral interference with absorption measurements and/or indirectly by either production of glyoxal on reaction with Teflon (walls of the chamber or sampling lines) or other VOCs in the chamber. In the first half of the experiment O$_3$ was injected into the chamber to three stable levels (0–2.5 ppmv) and then flushed out of the chamber (see Fig. S8). During these stable periods, the CE-DOAS and BBCEAS instruments changed the lengths of their sampling lines (adding new clean lengths of Teflon) to attempt to observe any change in the measured concentration. The only effect observed from longer Teflon lines was an increased amount of NO$_2$ (an increase of 60 pptv from 30–60 pptv NO$_2$ background) with longer sample lines caused by the reaction of O$_3$ with NO trapped at the surface of the tubing. In the second half of the experiment, attempts were made to observe glyoxal production in a dark, NO$_x$-free environment via reaction of OH with acetylene. The intention was to generate OH in the dark from the reaction of O$_3$ with 2,3-dimethyl-2-butene (tetramethylethylene, TME; ozonolysis OH yield of 0.90 – IUPAC recommendation). The chamber was left filled with 200 ppbv of O$_3$, acetylene (20 ppmv) was added and TME was shortly to be injected into the chamber (with the chamber roof closed). However, before the TME could be injected, rapid glyoxal production ensued with the glyoxal concentration reaching 45 ppbv over the following 3 h before the chamber was flushed clean (see Fig. S7a). The glyoxal is thought to have come from the reaction of O$_3$ with an impurity in the C$_2$H$_2$ (since several ppmv of C$_2$H$_2$ were added to the chamber an impurity with a relatively moderate yield of glyoxal would only have need to be 1 % of the C$_2$H$_2$ added). Several of these impurities were detected by FTIR in the 20 ppmv acetylene mixture inside the chamber, including 60 ppbv of ethene and 160 ppbv of acetone. The ozonolysis of ethene is known to produce OH (12–18 % yield, Chew and Atkinson, 1996) which then likely reacted with acetylene, which produces glyoxal as well as regenerate OH (30 % yield, Siese and Zetzsch, 1995; Bohn and Zetzsch, 1998).

3.2.6 Determination of precision, accuracy and detection limits

The data set presents an opportunity to assess precision, accuracy and detection limits of the various instruments while observing the same air mass. Experiment E8b investigated the overnight dilution of initially ~ 60 ppbv of glyoxal (4000 L min^{-1} flush rate) with all of the instruments mea-

suring continuously in their normal operating set up until the following morning. A time series of the data is shown in Figs. S8b and c. Several hours of data were collected in a flushed chamber where glyoxal and methyl glyoxal were both well below the detection limits of all of the instruments, but there may have been very small amounts of NO$_2$ and aerosol present. The expected glyoxal concentration during the targeted period (02:00–06:00 UTC; see gray area in Fig. S8c) was below 3 pptv based on the theoretical dilution. From these data histograms were constructed. From the Gaussian distributions of the histograms the standard deviation and mean were calculated for each instrument (see Fig. 9 for glyoxal and Fig. 10 for methyl glyoxal, the latter also using data from E8b after 02:00 UTC). The limit of detection (LOD) is defined as follows:

$$\text{LOD}_{\text{exp}} = 3 \cdot \sigma_{\text{Gaussian}} + |\text{background}|, \tag{7}$$

where the 1-σ variability was calculated during a period when the sensor signal is expected to be constant (E8b), and multiplied by 3; the "background" is taken as the absolute offset from the zero reference spectrum of the same time period (Figs. 9, 10 and S8). LOD as defined by Eq. (7) is widely used in analytical chemistry (IUPAC, 2006).

The experimental LODs are listed in Table 4 together with LOD values submitted with their measurement data by the operators of the various instruments. We find excellent agreement between the experimental LODs determined here and the reported LODs, once a common definition is applied. As seen in Figs. 9 and 10, the distributions are Gaussian (except for FTIR) and yielded LODs lower than or similar to the values reported for each instrument (see Table 4). For FT-IR the spread of data did not form a Gaussian distribution, and instead a simple average and standard deviation were calculated. All instruments performed within their specifications.

Accuracy represents the measurement uncertainty at high signal to noise (see Ryerson et al., 2013; Thalman and Volkamer, 2010). We assess accuracy from the variability in slopes relative to CE-DOAS, using only data from experiments where the maximum concentration is at least 10 times larger than the 1-σ variability deduced from E8b (LOQ, limit of quantification). The accuracy of the instruments was assessed from the difference between different methods at the 95 % CI level (see Table 4). See Sect. 4.2 for further discussions on LODs.

4 Discussion

4.1 UV-vis vs. IR absorption cross sections

The NCAR set of experiments compared three different calibration sources: (1) UV-vis absorption cross section, (2) infrared absorption cross section, and (3) PTR-ToF-MS activity related calibrations (from predicted reactivity of methyl glyoxal with H$_3$O$^+$). For glyoxal, the high-resolution UV-

visible cross section (Volkamer et al., 2005b) was adjusted to the instrument resolution of CE-DOAS by convolution with the instrument line-shape function (FWHM ~ 0.5 nm, characterized by the Hg atomic emission line at 435 nm or Cd lamp line at 480 nm). The UV absorption line strengths have previously been compared directly to IR line strengths by observing an identical gas-mixture in both spectral ranges simultaneously (Volkamer et al., 2005b). The integrated glyoxal IR cross sections near 2830 cm^{-1} (used to calibrate the EUPHORE FTIR) is 1.75×10^{-17} cm molecule^{-1} (base e, 2726–2922 cm^{-1}, see Profeta et al., 2011, for more details on energy ranges). The integrated glyoxal IR cross section near 1740 cm^{-1} (used to calibrate the NCAR FTIR) is 2.33×10^{-17} cm molecule^{-1}. This is 4.6 % higher than the values reported by Niki et al. (1985), 2.6 % higher than the integral IR cross section reported by Volkamer et al. (2005), and 1.6 % lower than the IR cross sections measured by Pacific Northwest National Laboratory (Profeta et al., 2011). The correlations for CE-DOAS and FT-IR (Table 3) from NCAR experiments agree within 2 ± 2 % at all temperatures (293–330 K). This excellent agreement demonstrates that the absolute cross sections in either spectral range are well known. We conclude that the uncertainty in the UV and IR spectral parameters is consistent with the error budget of 3 % uncertainty for absorption cross sections at the visible and IR spectral ranges (Volkamer et al., 2005b).

Measurements of methyl glyoxal in this study are calibrated using an integrated IR cross section of 7.88×10^{-18} cm molecule^{-1} near 2830 cm^{-1} to calibrate the EUPHORE FTIR, and 2.58×10^{-17} cm molecule^{-1} near 1740 cm^{-1} to calibrate the NCAR FTIR. Direct comparison of the EUPHORE and NCAR IR spectra showed a factor of 0.78 difference, which was traced to a near identical correction factor that had previously been applied to the EUPHORE-IR spectrum. This factor comes from the use of an older cross section (Raber, 1992) and cross calibration with the W-DOAS system. We note that the NCAR IR cross-section spectrum is 4 % lower than the IR cross section measured at Pacific Northwest National Laboratory (PNNL; Profeta et al., 2011), and further agrees well with other studies (Raber, 1992; Talukdar et al., 2011). After renormalization (eliminating the factor 0.78) the EUPHORE IR spectrum agrees well with the other IR spectra (Profeta et al., 2011; Talukdar et al., 2011). Further, the NCAR experiments provide a first temperature dependent cross-calibration of the vis- and IR spectral ranges for methyl glyoxal. The correlations for NCAR experiments find no evidence for a temperature effect, and slopes are unity with 1 % error. The vis spectrum by Meller et al. (1991) results in a near identical calibration for CE-DOAS as the above integral IR cross section for the NCAR FTIR. Finally, ion–molecule rate constant calculations for the reaction of methyl glyoxal with H$_3$O$^+$ result in slopes between PTR-ToF-MS and CE-DOAS of 0.93 ± 0.07 (i.e. indistinguishable from unity at the 95 % CI). Six independent sources of calibration are there-

fore consistent within 5 %, which we interpret as an upper limit for the uncertainty in the vis- and IR cross sections of methyl glyoxal, and as the uncertainty in the ion–molecule rate constant (rate $= 1.47 \times 10^{-9}$ cm^3 s^{-1}). Based on a careful comparison of the available spectra, we recommend the following integrated infrared cross section values for use in future studies: $(2.86 \pm 0.14) \times 10^{-17}$ cm molecule^{-1} between 1600 and 1800 cm^{-1} (average of NCAR, PNNL, Profeta et al., 2011, and NOAA spectra, Talukdar et al., 2011,); $(9.9 \pm 0.5) \times 10^{-18}$ cm molecule^{-1} between 2780 and 2880 cm^{-1} (average of PNNL and NOAA spectra). The recommended values include an estimated overall uncertainty of 5 %.

4.2 Precision, accuracy, and limit of detection

Different practices to estimate LOD can lead to a factor of 6 difference between LOD values reported in the literature (Thalman and Volkamer, 2010) due to notation, rather than differences in the figure of merit characteristic of an instrument. The simultaneous observation of a common air mass facilitates calculation of LOD using a consistent definition, i.e., Eq. (7) applied across all instruments. The methods underlying LOD reports vary because of the different information provided from the different instruments. For single-channel instruments (e.g., fluorescence, chemiluminescence, phosphorescence, and voltammetry), the 1-σ variability at constant signal is widely used to characterize "precision" ($=$ the 3-σ component of Eq. 7). For multi-channel sensors the fit-error from spectral fitting is indirectly related to, but not identical to, the variability. Multi-channel (spectral) sensors can further leverage additional information, for example, accounting for systematic residual structures that may remain after all known absorbers have been accounted to inform on the potential for systematic bias due to spectral cross-correlation (Stutz and Platt, 1996). This has resulted into more conservative reports of LOD from some multispectral sensors (see Sect. 4 in Thalman and Volkamer, 2010). Ultimately, assessing the accuracy of an instrument requires the comparison to other instruments.

Table 4 illustrates that the offsets in clean air contribute significantly to the LOD. For instruments where the scatter behaves statistical (i.e., Gaussian distributions in Figs. 9 and 10), the precision can be improved by averaging data in time. While the background varies significantly between instruments, we find that at ~ 4 min averaging time the contributions due to precision and "background" to the overall LOD$_{\text{Eq. (7)}}$ become roughly comparable for Mad-LIP, BBCEAS and CE-DOAS. Further averaging has limited potential to reduce LOD further, unless active measures are also taken to minimize "background". The factors that determine "background" contributions vary in different instruments, and deserve further investigation. For example, the CE-DOAS offset in Figs. 9 and 10 is for data that used a nearby reference spectrum; the choice of a different refer-

ence spectra from the start and/or end of the experiment can lead to offsets of 8 pptv over 24 h; we have combined the offset over 24 h in quadrature to obtain a conservative estimate of the contribution from "background" for CE-DOAS in Table 4, see also Sect. 4.6 for further discussion.

We note that all instruments during EUPHORE experiments were either calibrated directly or indirectly from the same UV-visible cross section (Volkamer et al., 2005b). This calibration is directly accomplished by fitting the convolved literature cross sections for W-DOAS, CE-DOAS and BBCEAS. Calibration is less direct for FTIR (cross-section calibrated to the W-DOAS, SPME calibrated to the FTIR). Mad-LIP is calibrated by flowing a calibration gas through a ring-down cell while monitoring the 440 nm absorption feature, and into the LIP instrument; UV-visible absorption by the ring-down cell is calibrated from the glyoxal or methyl glyoxal UV-visible cross section. By relating all instruments to a common source of calibration information the experiments at EUPHORE eliminate potential for calibration bias, and isolate other (unknown) factors that may limit accuracy. The observed variability in slopes between experiments is usually larger than the uncertainty in the cross section (see Sect. 4.1.). The 95 % confidence intervals of slopes are listed in Table 4 for all instruments (relative to CE-DOAS) as a measure of accuracy at high signal-to-noise. This was done by averaging these slopes relative to CE-DOAS for each instrument and assessing the confidence interval of this sample of slopes (thus omitting experiments where the correlation does not include a maximum value of at least 10 times the 1-σ detection limit). It is generally smallest (4–7 %) for absorption instruments, and larger for Mad-LIP (glyoxal: average slope = 1.06 ± 0.53; methyl glyoxal: average slope = 1.80 ± 0.58), SPME (glyoxal: average slope = 1.14 ± 0.53; methyl glyoxal: average slope = 0.75 ± 0.18) and PTR-ToF-MS (1.23, only one measurement).

For the Mad-LIP, instrument problems caused by the initially low flows prevented noticing that the multi-pass optics in the LIP cell were degraded. Testing after the field campaign confirmed that mirror degradation had a two-fold effect in that the background scatter was increased and the effective laser-power reduced. Both factors reduce the LOD explaining the difference between the LOD reported in Henry et al. (2012) and the value in Table 4. The variability of the slope of the LIP instrument is attributed to alignment variations of the multi-pass cell. Changes in alignment affect the net laser power in the detection volume and are hard to account for. Such alignment changes resulted from the instrument maintenance performed during the intercomparison as part of the diagnostics of the flow problems and the low detection limit. Based on the results of this intercomparison a new version of Mad-LIP is using a single-cell detection axis with comparable detection efficiency but much greater stability (as demonstrated for LIF measurement of formaldehyde, Cazorla et al., 2015).

4.2.1 Choice of reference instrument

Both CE-DOAS and BBCEAS were considered as reference techniques. We chose CE-DOAS to assess relative differences to other instruments for the following reasons: (1) the instrument participated in both campaigns, (2) had excellent data coverage, and (3) high time resolution. Use of CE-DOAS yields the maximum number of data points to calculate correlations between different instruments at EUPHORE. Further, (4) CE-DOAS demonstrated the lowest LOD$_{Eq. (7)}$, and concentration offsets for both glyoxal and methyl glyoxal among all available instruments (see Table 4, Figs. 9 and 10); (5) CE-DOAS benefits from inherent path length calibration through O$_4$ at very high signal-to-noise to demonstrate control over cavity alignment with very little error (2 %). (6) The comprehensive coverage and consistent performance from CE-DOAS in context with the other instruments that we compared at both chamber facilities provides strong evidence to suggest CE-DOAS is precise, and accurate. (7) The size of white-noise residuals observed by CE-DOAS can be understood in terms of the measured photon fluxes, and provides additional information to assess LOD and accuracy (Sect. 3.2.6, Fig. S9). The Supplement contains a discussion of potential sources for systematic bias with CE-DOAS measurements. At high concentrations the resulting error of 3.5 % is dominated by the uncertainty in the absorption cross sections. A discussion of the factors that influence accuracy at low concentrations is provided in Sect. 4.6.

4.3 Interference from biacetyl and O$_3$

Biacetyl is formed simultaneously with glyoxal and methyl glyoxal in a complex array of other ring opening and retaining products in the photo-oxidation of o-xylene. We did not observe any measurable interference in detection of glyoxal and methyl glyoxal from biacetyl up to $\sim$ 2 ppbv (estimated from model simulation of the chamber reaction and known yields) during experiment E3. Most instrument slopes agreed within 10 % for glyoxal, and differences of $\sim$ 20 % for Mad-LIP cannot be explained by biacetyl signals, which would result in larger than unity slopes. BBCEAS, CE-DOAS and W-DOAS are expected to be insensitive to interference from biacetyl, due to its relatively unstructured absorption cross section (see Fig. S1) and the fact that the selectivity of retrievals arises from differential absorption structures (prominent for glyoxal). Similarly, sensitivity for biacetyl by Mad-LIP had been tested previously and the lack of sensitivity (no phosphorescence) due to quenching by oxygen is consistent with findings in this study (Henry et al., 2012).

The hypothesis for this experiment was that the structure of the biacetyl absorption cross- section (Fig. S1) could cause interferences for other α-dicarbonyls. For methyl glyoxal, BBCEAS and SPME during experiment E3 were 8 and 13 %, respectively, lower than CE-DOAS, while FTIR and

Mad-LIP showed slopes that were 30 and 70 % higher. For FTIR, this positive bias appears to be twice as high as during experiment E2, the only other methyl glyoxal comparison available. We note that methyl glyoxal concentrations of 8 and 12 ppbv for FTIR and Mad-LIP (see Fig. 7), respectively, during experiment E3 are only 2–3 times above the FTIR detection limit. Thus the difference of 15 % compared to E2 can probably (at least) partially be explained by systematic bias of FTIR near the detection limit as well as the complex mixture in the chamber for photo-oxidation experiments including the incomplete subtraction of water bands in the FTIR. SOA formation is unlikely to affect the optical measurements; scattering is inefficient at IR wavelengths, and a filter removes SOA in the CE-DOAS sampling line. The positive difference in slope observed for Mad-LIP currently remains unexplained. Previous cross sensitivity tests did not show a measurable sensitivity of methyl glyoxal signals towards biacetyl (Henry et al., 2012). We note that E6 and E7 revealed a similar or larger bias in slopes for Mad-LIP methyl glyoxal, but no biacetyl was present during E7. Hence, the differences for Mad-LIP methyl glyoxal are likely due to other reasons, and cross interference from biacetyl is difficult to judge from this data set.

The SPME results did not show a clear trend of a bias of glyoxal and methyl glyoxal, and were found highly variable during this comparison exercise. The SPME sampling carried out during the intercomparison exercise suffered from manual manipulation and possible contamination in the period after sampling from the chamber and desorption in the GC. This effect could be more evident when measuring lower concentrations. After the campaign, an automated system has been implemented to eliminate manual manipulation and has enabled the improvement of the SPME system (Borrás et al., 2015).

In experiment E5 the only effect of flowing O_3 was the conversion of some of the NO trapped on/in the Teflon into NO_2 that varied with the length of the inlet line. No other effect on the methyl glyoxal or glyoxal signals were observed due to O_3. It should be noted that various groups had observed that O_3 flowing in Teflon (PFA) tubing can be a source for glyoxal (observed by CU-Boulder and UW-Madison for some limited sets of tubing). However, the effect of O_3 is usually only visible at very small glyoxal concentrations (< 20 pptv). A more comprehensive and systematic study on the role of O_3 at very low glyoxal concentrations warrants future research.

4.4 Interference from NO_2

Elevated NO_2 concentrations did show an effect on the concentrations of glyoxal and methyl glyoxal determined by the cavity-based instruments (CE-DOAS and BBCEAS, but not for Mad-LIP glyoxal). We quantify the bias due to NO_2 as ca. 1 pptv glyoxal/ppbv NO_2 (Fig. 4) and 5 pptv methyl glyoxal/ppbv NO_2 (Fig. S3), though the effect does not have a

clear trend (see Fig. 5) and is generally smaller than the uncertainty in the measurements. The primary effects of high NO_2 (> 10 ppbv) are due to NO_2 light extinction. This limits the attainable effective absorption path lengths, and removes photons, thus further increasing photon shot noise. All of these effects lead to increasing uncertainty for measured glyoxal and methyl glyoxal. For CE-DOAS ($R = 0.999972$) 200 ppbv of NO_2 changes the sample path length from 15 to 3.5 km and the light throughput is reduced by a factor 4. The combined effect is a decrease of a factor of 8 in sensitivity. For BBCEAS the effects are similar, but the reduction in path length is from 5 to 2.3 km (a factor of 2). At the highest level of NO_2 ($\sim$ 200 ppbv) the absorption due to NO_2 is more than 500 times greater than that due to 0.3 ppbv of glyoxal used in E9 (Fig. 4) and more than 300 times greater than for 6 ppbv of methyl glyoxal used in E10 (Fig. S3). The largest effect of the NO_2 is the differential absorption structure. This creates residual structures that make DOAS retrievals difficult for all of the visible light absorption techniques (W-DOAS, CE-DOAS and BBCEAS). This also creates a highly structured absorption path length in the cavity based instruments (CE-DOAS and BBCEAS) as the extinction due to NO_2 begins to determine the cavity light path. For instance, the variation in the absorption path length for CE-DOAS is 35 % over the space of 3 nm with 200 ppbv of NO_2 in the instrument. Despite this difference in the differential absorption, the very small biases in glyoxal and methyl glyoxal due to NO_2 is indeed surprising, and encouraging. The Mad-LIP glyoxal measurements are unaffected by large amounts of NO_2. The FTIR showed a slight increase in the methyl glyoxal signal relative to the SF_6 tracer (Fig. S3) although all FTIR methyl glyoxal data points agreed comfortably (within their error bars) with the SF_6 dilution trend. The glyoxal concentrations used in E9 were below the FTIR detection limit. The W-DOAS instrument may be similarly affected by large fitting residuals due to NO_2, but the glyoxal and methyl glyoxal concentrations used in E9 and E10 were at or below the detection limit. The Mad-LIP was off-line for the methyl glyoxal experiment. For the SPME the reported concentrations varied too widely to evaluate the interference.

For ambient NO_2 concentrations smaller than 10 ppbv, the effect on glyoxal retrievals is primarily due to uncertainties in the absorption cross section. An interesting subset of data from E6 is the time from when the experiment was started and ambient air is introduced until noon. During this time, glyoxal was generally below 0.5 ppbv, and NO_2 varied between 2 and 15 ppbv. Under these conditions, glyoxal correlations between CE-DOAS and BBCEAS and Mad-LIP are shown in Fig. S5, and the slopes/intercepts/R^2 values are given in Table 5. The differences between glyoxal as measured by the absorption techniques were calculated by subtracting the Mad-LIP concentration, and this Δglyoxal is shown in Fig. S6 as a function of NO_2. A regression analysis confirms the results obtained during E9 in ambient air (CE-DOAS: $-1.1(8)$ pptv glyoxal/ppbv NO_2; see also

Table 5. Correlations at ambient (sub-ppbv) glyoxal concentrations: BBCEAS, Mad-LIP, and CE-DOAS (reference) data.

Exp #	Species	Instrument	# pts	Slope	Int. (ppbv)	R^2	Range (ppbv) glyoxal	NO$_2$	RH (%)
Pure compound experiments									
E1[a]	GLY	BBCEAS	478	0.96(1)	−0.002(2)	0.99	0–0.3	<1	<1
E1[a]	GLY	Mad-LIP	223	1.08(4)	−0.014(2)	0.89	0–0.3	<1	<1
E8a	GLY	BBCEAS	256	1.03(3)	−0.013(2)	0.97	0–0.3	<1	<1
E8a	GLY	Mad-LIP	136	1.23(6)	−0.010(5)	0.98	0–0.3	<1	<1
E8b	GLY	BBCEAS	315	0.97(3)	−0.022(2)	0.95	0–0.3	<1	<1
E8b	GLY	Mad-LIP	321	1.20(3)	0.012(3)	0.98	0–0.3	<1	<1
Mixed compound experiments									
E3	GLY	BBCEAS	191	1.02(4)	−0.011(4)	0.97	0–0.3	0–4	2
E6[b]	GLY	BBCEAS	231	0.98(3)	−0.027(8)	0.91	0–0.5	0–16	30–50
E6[b]	GLY	Mad-LIP	87	1.02(5)	−0.011(11)	0.97	0–0.5	0–16	30–50
E7	GLY	BBCEAS	61	1.01(6)	−0.10(2)[c]	0.99	0–0.3	0–13	38
E7	GLY	Mad-LIP	123	1.38(18)	−0.10(7)[c]	0.98	0–0.3	0–13	38

[a] Experiment E1 data is from the morning of 24 June; ∼ 1 ppbv NO$_2$ and 3 ppbv methyl glyoxal were injected into the chamber with an impure glyoxal sample at low concentration. [b] E6 correlations are for concentrations below 500 pptv. See Figs. S5 and S6 for explanation of the deviation in the Mad-LIP fit here due to inhomogeneity of the chamber. [c] Intercepts here are due to chamber homogeneity (Fig. S10).

Fig. S6). These results show little to no effect of NO$_2$ levels below 10 ppbv on ambient glyoxal concentrations (here below 500 pptv).

4.5 Interference from H$_2$O

Absorption by gas-phase water overlaps with the glyoxal, methyl glyoxal and NO$_2$ absorption in the UV/VIS spectral range. The available spectral databases like HITRAN have considerable uncertainties in this spectral range, and are subject to ongoing updates in recent HITRAN/HITEMP data products (Rothmann et al., 2010, 2013). The effect of water on glyoxal retrievals depends on the absolute amount of water present in the gas-phase. This was investigated systematically during experiments E6 and E7. The humidity during E6 (30–50 % RH at 303 K) corresponds to 2.1 %$_{v/v}$ H$_2$O, or 15.2 g m^{-3} absolute humidity. This is 5.5 and 1.6 times higher than the absolute humidity of 2.76 and 9.65 g m^{-3} at 50 % RH at 275 and 295 K that is characteristic of the arctic-, and mid-latitude troposphere; and somewhat lower than humidity in tropical air (26.9 g m^{-3}; 80 % RH at 305 K). In principle also other unknown factors in the ambient air studied during E6 could affect the retrievals; however, for the absorption techniques, H$_2$O is the primary and the only known factor. In particular, NO$_2$, O$_3$, and aerosols can be ruled out to influence the glyoxal retrievals during E6 (see Table 3, Sects. 3.2.3, 3.2.4, 4.3, and 4.4). Tables 3 and 5 do not provide evidence that would suggest a significant specific influence of H$_2$O absorption on glyoxal retrievals.

At ambient glyoxal concentrations, three of the four participating instruments had sufficient sensitivity to provide meaningful low error bars (Table 5, also Sect. 4.6). The BBCEAS, Mad-LIP, and CE-DOAS instruments generally agree within 5–20 % under both dry (E1, E3, E5, E8a) and moist conditions (E6, E7). At high absolute humidity agreement as good as 5 % is observed between all three instruments. Larger differences were sometimes observed (up to 35 %), and are influenced by lower signal-to-noise due to lower concentrations (Sect. 4.6). There is no obvious systematic behavior between the three instruments that would suggest a specific H$_2$O effect. The magnitude of intercepts was generally smaller than the LOD (compare Table 4), and the quality of correlations ($0.80 < R^2 < 0.94$) did not show an obvious dependence on gas-phase H$_2$O. A recent study compared an advanced instrument version (Coburn et al., 2014) of the CE-DOAS used in this study with two ship- and aircraft-based remote-sensing techniques at lower glyoxal (∼ 35 pptv) and higher humidity in the remote tropical marine boundary layer (Volkamer et al., 2015). The choice of H$_2$O cross section introduced ∼ 13 % bias for glyoxal (and ∼ 16 % bias for iodine monoxide, IO), which corresponds to an offset of ∼ 5 pptv glyoxal, or 1–5 % at 500 and 100 pptv, respectively. Such sensitivity is generally consistent with the findings in this work, and it is below the LOD of instruments used in this study (Tables 4 and 5), suggesting water effects are small, and do not pose a fundamental limitation also at ambient concentrations. We conclude that better knowledge of the water absorption cross sections at blue wavelengths is needed to eliminate residual absorption effects due to water's bands. This has potential to help further improve the detec-

tion sensitivity by absorption techniques, and eliminate small potential for bias at ambient glyoxal concentrations. Furthermore, RH more than absolute humidity determines the partitioning of glyoxal and methyl glyoxal to aerosols, aerosol filters, and the walls of sampling lines (Sect. 3.2.5). A systematic study of RH effects at different temperatures has not been attempted, because temperature (and RH) cannot easily be controlled independently at EUPHORE.

4.6 Comparison of atmospheric glyoxal concentrations

The BBCEAS, Mad-LIP, and CE-DOAS instruments had sufficient sensitivity to provide meaningful low error bars at ambient glyoxal concentrations. Table 5 compiles the correlations for periods of the experiments when glyoxal was generally less than 300 pptv, and always smaller than 500 pptv for E6 and E7. The comparison of data in Table 5 was limited to periods when the chamber was regarded as homogeneous, and glyoxal varied sufficiently to allow for a meaningful regression analysis. If these factors are considered, the slopes varied between 0.96 and 1.38 (E8a, E8b, E3, E6, E7, Table 5). The variability of slopes at low concentrations (pure: 0.96–1.23, mixed: 0.98–1.38, Table 5) was actually smaller than at high concentrations (pure: 0.68–1.43; mixed: 0.68–2.21, Table 3) for the same instruments. The intercepts were below the instruments' respective LODs, and the quality of correlations was generally very good; as was the case at high concentrations, R^2 values were slightly better for pure compound experiments. Overall, the surprisingly good agreement suggests a reliable quantification of ambient glyoxal concentrations (within the respective errors, Table 4).

Notably, the experiments were initially designed for measurements by all instruments, and not specifically optimized for comparisons at low concentrations; in particular parts of the data in E5, E6 and E7 suffer from inhomogeneity in the chamber air during the period when ambient air was added (as can be seen in Fig. S10). The larger negative intercepts in E7 are caused by the chamber inhomogeneity as the CE-DOAS responds to the opening of the chamber roof and the start of the photochemistry before the BBCEAS and Mad-LIP. At low concentrations, the lower signal to noise is starting to limit the overall accuracy (not better than LOD$_{\text{Eq. (7)}}$ in Table 4). At 150 pptv glyoxal (typical semi-polluted concentration), limitations due to signal-to-noise account for ∼ 10 % uncertainty in CE-DOAS and ∼ 30 % in BBCEAS, which is 3–6 times higher than the uncertainty at high signal to noise (see column "accuracy" in Table 4). Baseline drift can further limit LOD as it adds to the "background" in Eq. (7). Such offset can be caused by instrument instabilities (e.g., intensity variations in the LED for absorption techniques), and the non-linear calibration curve for the Mad-LIP. Baseline drift becomes relatively more important at low concentrations; e.g., an offset of 20 pptv (see Fig. 9) corresponds to 16 % at 150 pptv glyoxal. For the spectroscopic instruments (absorption measurements) this "background" value

(see Eq. 7) can be reduced by more frequent acquisition of reference spectra (see Sect. 4.2). For Mad-LIP this offset can be reduced by more frequent calibrations.

4.7 Relevance for measurements in the atmosphere

Our results show that advances with measurement techniques in recent years are suitable to attempt the detection of glyoxal at ambient mixing ratios in polluted urban (up to 1.5 ppbv, Volkamer et al., 2005), semi-polluted rural air (100–500 pptv, Washenfelder et al., 2011; Knote et al., 2014), forests (0.25–1.5 ppbv, Huisman et al., 2011), marine boundary layer (20–50 pptv, Sinreich et al., 2010; Coburn et al., 2014; Volkamer et al., 2015) and the free tropospheric environments (3–30 pptv, Lee et al., 1998; Baidar et al., 2013; Volkamer et al., 2015). In most urban environments the glyoxal detection by in situ UV-vis absorption techniques is feasible; i.e., there is no fundamental limitation due to typical ambient NO$_2$ concentrations. However, care must be taken with accurately characterizing the effect of NO$_2$ on the effective absorption paths, and the representation of overlapping absorption features during retrievals. Several optical techniques now facilitate the fast (few Hz) in situ detection of glyoxal. Such time resolution is suitable to conduct measurements from mobile platforms such as aircraft, or for micro-meteorological flux calculations. The first eddy covariance flux measurements of glyoxal have recently been demonstrated by CE-DOAS over the remote ocean (Coburn et al., 2014).

Measurements of methyl glyoxal in the atmosphere are complicated by its short atmospheric lifetime (∼ 0.5–1 h). As a result, ambient mixing ratios are comparable and often lower than those of glyoxal under polluted urban (0.1–2 ppbv, Grosjean et al., 1996; Okuzawa et al. 2007), biogenic and background regions (0–1 ppbv, Kawamura et al., 2013; Matsunaga et al., 2004; Ieda et al., 2006) or during biomass burning events (0.5–3 ppbv, 2010 Boulder, CO 4-mile fire, Thalman, 2013). Detection by optical absorption techniques at UV-vis wavelengths has limited sensitivity since the absorption cross section of methyl glyoxal is ∼ 10 times lower compared to glyoxal; at IR wavelengths the combination of low cross sections and spectral overlap with other species complicates measurements of low ambient concentrations of methyl glyoxal. Detection by phosphorescence is complicated by significant interferences from glyoxal that renders calibration factors too strong a function of environmental conditions to facilitate a meaningful quantification of methyl glyoxal in the presence of glyoxal. Detection by PTR-ToF-MS has the issue of coincidental masses from reaction intermediates, H$_3$O$^+$ reagent ion clusters and the fragmentation of larger compounds upon protonation in the mass spectrometer. There still remains a need to develop highly time-resolved on-line measurements of methyl glyoxal at ambient mixing ratio levels.

5 Conclusions

Nine different instruments measuring α-dicarbonyls were compared during two separate intercomparison campaigns (3 at NCAR, 7 at EUPHORE; CE-DOAS participated in both campaigns). The nine instruments used three independent sources of calibration (see Sect. 4.1), and additional comparisons with calibrations of literature cross-section data were conducted. Systematic bias between techniques was eliminated by observing the same air volume, and calibration bias was minimized as far as possible by relating the calibrations of most instruments at EUPHORE (except the PTR-ToF-MS for methyl glyoxal) to the UV-vis absorption cross sections available in the literature. We conclude

- The absorption cross-section spectra for glyoxal and methyl glyoxal at visible and IR wavelengths are robust. Simultaneous measurements at visible and IR wavelengths agree within $2 \pm 3\%$ for glyoxal, and within $1 \pm 4\%$ for methyl glyoxal. No evidence is found for a temperature effect over the range from 293 to 330 K in either glyoxal or methyl glyoxal cross sections. Further, the NCAR PTR-ToF-MS calibration based on a theoretical calculation of the proton affinity of methyl glyoxal agrees with visible and IR calibrations within 5 %.

- Seven instruments at EUPHORE used a common source for calibration from the same UV-visible spectrum for glyoxal (Volkamer et al., 2005b) and methyl glyoxal (Meller et al., 1991). We find excellent linearity between all instruments under idealized conditions (pure glyoxal or methyl glyoxal, $R^2 > 0.96$), and in complex gas mixtures characteristic of dry photochemical smog systems (o-xylene/NO$_x$ and isoprene/NO$_x$, $R^2 > 0.95$; $R^2 \sim 0.65$ for offline SPME measurements of methyl glyoxal). The correlations are slightly more variable in humid ambient air mixtures (RH $> 45\%$) for methyl glyoxal ($0.58 < R^2 < 0.68$) than for glyoxal ($0.79 < R^2 < 0.99$).

- The intercepts of correlations were largely found to be insignificant (below experimentally determined detection limits), and slopes varied by less than 5 % for NO$_2$. For glyoxal and methyl glyoxal the slopes varied by 12 and 17 % (3-σ), respectively, between inherently calibrated instruments (i.e., direct calibration from the absorption cross section). A larger variability is found among techniques that employ external calibration sources (75–90 %, 3-σ), and/or offline analysis (SPME); we identify $\sim 80\%$ high-bias in Mad-LIP measurements of methyl glyoxal (see Sect. 2.1.6 and 4.2). Instrument specific differences are 4–20 times larger than the uncertainty in the cross sections. We conclude that the accuracy of calibration procedures can introduce systematic bias as large as a factor of 2 for both glyoxal and methyl glyoxal.

- Differences in reports about precision and detection limits (LOD) in the literature are evaluated (Sect. 4.2, Table 4). The accuracy of instruments is found to vary between 3.5 % and up to a factor of 2, depending on the instrument and species.

Comparison of Mad-LIP, BBCEAS and CE-DOAS at ambient glyoxal concentrations (0–500 pptv) gave the following results

- Offset concentrations can dominate over instrument precision and limit the attainable overall LOD$_{Eq.\ (7)}$ (Table 4) for few minutes of averaging (all instruments). The observed offsets for glyoxal were smaller 10 pptv (CE-DOAS, BBCEAS), and ~ 25 pptv (Mad-LIP). Attempts to lower LOD$_{Eq.\ (7)}$ by temporal averaging of data reduced the statistical noise, but required active steps to reduce "background" signal. For example, CE-DOAS offset drift was smaller 2 pptv over several hours by using a nearby reference spectrum, and ~ 8 pptv using a 24 h shifted reference spectrum. The frequency of recording reference spectra (absorption techniques) and calibrations (Mad-LIP) can help reduce/characterize offset concentrations, and should be optimized to balance competing objectives to either lower LOD and/or ensure the highest possible precision/accuracy for the respective experimental/ambient conditions.

- The presence of NO$_2$ had a surprisingly small effect on glyoxal and methyl glyoxal retrievals. For NO$_2$ below 10 ppbv, no effect was noticeable. At higher NO$_2$ (< 200 ppbv were tested), the systematic bias was characterized as ~ 1 pptv glyoxal/ppbv NO$_2$, and ~ 5 pptv methyl glyoxal/ppbv NO$_2$ for CE-DOAS and BBCEAS (SF$_6$ dilution tracer as reference technique). Pure and mixed compound experiments gave similar results.

- The addition of water vapor (H$_2$O) on glyoxal retrievals was tested up to a specific humidity of 15.2 g m^{-3}. Residual structures due to imperfect knowledge of H$_2$O absorption cross sections in HITRAN did not result in noticeable bias (< 5 pptv) for ambient glyoxal concentrations (Table 5, Sect. 4.6), but limit the attainable sensitivity. Slightly larger effects were observed for methyl glyoxal at higher concentrations (Sect. 3.2.4). At moderate relative humidity ($\sim 50\%$ RH), no evidence is found that glyoxal or methyl glyoxal is removed by aerosol filters placed into sampling lines, if these filters are changed routinely, based on the good agreement of CE-DOAS (filtered) and BBCEAS (unfiltered).

- Similarly, the addition of O$_3$, or biacetyl under atmospherically relevant concentrations had no noticeable effect.

Future studies should investigate in detail the small offset concentrations for α-dicarbonyls in the instruments (back-

ground variability/history of system). This includes the effect of O_3, H_2O, RH and sampling line history in experiments that sample very low concentrations of α-dicarbonyls ($\sim$ 20–50 pptv). At high relative humidity ($>80\%$ RH) losses/formation in sampling lines or to/from aerosol filters are likely to be more relevant. Any future instrument intercomparison experiments should be planned to decouple the influence of temperature and relative humidity, and ideally investigate a broader range of synthetic and ambient mixtures including standard addition type experiments with ambient air and small additions of the target compound. Further, better knowledge about the absorption cross section of H_2O is needed. While the bias due to H_2O residual absorption in the visible spectral range (420–470 nm) is likely small for glyoxal, the uncertainty about H_2O cross-sections limits the attainable detection sensitivity. Finally, there is a need to develop fast on-line measurement techniques capable of detecting selectively methyl glyoxal at low ambient concentrations (LOD of $\sim$ 10 pptv methyl glyoxal is desirable for routine ambient detection).

The Supplement related to this article is available online at doi:10.5194/amt-8-1835-2015-supplement.

References

Ahlm, L., Liu, S., Day, D. A., Russell, L. M., Weber, R., Gentner, D. R., Goldstein, A. H., DiGangi, J. P., Henry, S. B., Keutsch, F. N., VandenBoer, T. C., Markovic, M. Z., Murphy, J. G., Ren, X., and Scheller, S.: Formation and growth of ultrafine particles from secondary sources in Bakersfield, California, J. Geophys. Res., 117, D00V08, doi:10.1029/2011JD017144, 2012.

Alvarez, E. G. and Valcárcel, M.: Research into conditions of quantitivity in the determination of carboniles in complex air matrices by adsorptive solid phase microextraction, Talanta, 77, 1444–1453, 2009.

Baidar, S., Oetjen, H., Coburn, S., Dix, B., Ortega, I., Sinreich, R., and Volkamer, R.: The CU Airborne MAX-DOAS instrument: vertical profiling of aerosol extinction and trace gases, Atmos. Meas. Tech., 6, 719–739, doi:10.5194/amt-6-719-2013, 2013.

Baker, J., Arey, J., and Atkinson, R.: Formation and reaction of hydroxycarbonyls from the reaction of OH radicals with 1,3-butadiene and isoprene, Environ. Sci. Technol., 39, 4091–4099, 2005.

Ball, S. M., Hollingsworth, A. M., Humbles, J., Leblanc, C., Potin, P., and McFiggans, G.: Spectroscopic studies of molecular iodine emitted into the gas phase by seaweed, Atmos. Chem. Phys., 10, 6237–6254, doi:10.5194/acp-10-6237-2010, 2010.

Bao, M. L., Pantani, F., Griffini, O., Burrini, D., Santianni, D., and Barbieri, K.: Determination of carbonyl compounds in water by derivatization – solid-phase microextraction and gas chromatographic analysis, J. Chromatogr. A, 809, 75–87, 1998.

Becker, K. H. (Ed.): The European Photoreactor EUPHORE, Final Report of the EC-Project EUPHORE, Contract EV5VCT92-0059, Bergische Universität Wuppertal, Dept. of Chemistry, Germany, 1996.

Blake, R. S., Monks, P. S., and Ellis, A. M.: Proton-transfer reaction mass spectrometry, Chem. Rev., 109, 861–896, 2009.

Bohn, B. and Zetzsch, C.: Formation of HO_2 from OH and C_2H_2 in the presence of O_2, J. Chem. Soc., 94, 1203–1210, doi:10.1039/A708536B, 1998.

Borrás, E., Muñoz A., Ródenas M., and Vera, T.: in preparation, 2015.

Coburn, S., Ortega, I., Thalman, R., Blomquist, B., Fairall, C. W., and Volkamer, R.: Measurements of diurnal variations and eddy covariance (EC) fluxes of glyoxal in the tropical marine boundary layer: description of the Fast LED-CE-DOAS instrument, Atmos. Meas. Tech., 7, 3579–3595, doi:10.5194/amt-7-3579-2014, 2014.

Cazorla, M., Wolfe, G. M., Bailey, S. A., Swanson, A. K., Arkinson, H. L., and Hanisco, T. F.: A new airborne laser-induced fluorescence instrument for in situ detection of formaldehyde throughout the troposphere and lower stratosphere, Atmos. Meas. Tech., 8, 541–552, doi:10.5194/amt-8-541-2015, 2015.

Chew, A. A. and Atkinson, R.: OH radical formation yields from the gas-phase reactions of O_3 with alkenes and monoterpenes, J. Geophys. Res., 101, 28649–28653, doi:10.1029/96JD02722, 1996.

Daniels, M. J. S. and Ball, S. B.: in preparation, 2015.

de Gouw, J. and Warneke, C.: Measurements of volatile organic compounds in the earth's atmosphere using proton-transfer-reaction mass spectrometry, Mass Spectrom. Rev., 26, 223–257, 2007.

de Gouw, J. A., Goldan, P. D., Warneke, C., Kuster, W. C., Roberts, J. M., Marchewka, M., Bertman, S. B., Pszenny, A. A. P., and Keene, W. C.: Validation of proton transfer reaction-mass spectrometry (PTR-ToF-MS) measurements of gas-phase organic compounds in the atmosphere during the New England Air Quality Study (NEAQS) in 2002, J. Geophys. Res., 108, 4682, doi:10.1029/2003JD003863, 2003.

DiGangi, J. P., Henry, S. B., Kammrath, A., Boyle, E. S., Kaser, L., Schnitzhofer, R., Graus, M., Turnipseed, A., Park, J-H., Weber, R. J., Hornbrook, R. S., Cantrell, C. A., Maudlin III, R. L., Kim, S., Nakashima, Y., Wolfe, G. M., Kajii, Y., Apel, E.C., Goldstein, A. H., Guenther, A., Karl, T., Hansel, A., and Keutsch, F. N.: Observations of glyoxal and formaldehyde as metrics for the anthropogenic impact on rural photochemistry, Atmos. Chem. Phys., 12, 9529–9543, doi:10.5194/acp-12-9529-2012, 2012.

Dubé, W. P., Brown, S. S., Osthoff, H. D., Nunley, M. R., Ciciora, S. J., Paris, M. W., McLaughlin, R. J., and Ravishankara, A. R.: Aircraft instrument for simultaneous, in situ measurement of NO$_3$ and N$_2$O$_5$ via pulsed cavity ring-down spectroscopy, Rev. Sci. Instrum., 77, 34101–34111, 2006.

Ervens, B. and Volkamer, R.: Glyoxal processing by aerosol multiphase chemistry: towards a kinetic modeling framework of secondary organic aerosol formation in aqueous particles, Atmos. Chem. Phys., 10, 8219–8244, doi:10.5194/acp-10-8219-2010, 2010.

Ervens, B., Carlton, A. G., Turpin, B. J., Altieri, K. E., Kreidenweis, S. M., and Feingold, G.: Secondary organic aerosol yields from cloud-processing of isoprene oxidation products, Geophys. Res. Lett., 35, L02816, doi:10.1029/2007GL031828, 2008.

Fayt, C. and Van Roosendael, M.: WinDOAS User Manual, Belgian Institute for Space Aeronomy, Brussels, Belgium, 2001.

Feierabend, K. J., Zhu, L., Talukdar, R. K., and Burkholder, J. B.: Rate coefficients for the OH + HC(O)C(O)H (glyoxal) reaction between 210 and 390 K, J. Phys. Chem. A, 112, 73–82, 2007.

Fu, T. M., Jacob, D. J., Wittrock, F., Burrows, J. P., Vrekoussis, M., and Henze, D. K.: Global budgets of atmospheric glyoxal and methylglyoxal, and implications for formation of secondary organic aerosols, J. Geophys. Res., 113, D15303, doi:10.1029/2007JD009505, 2008.

Galloway, M. M., Chhabra, P. S., Chan, A. W. H., Surratt, J. D., Flagan, R. C., Seinfeld, J. H., and Keutsch, F. N.: Glyoxal uptake on ammonium sulphate seed aerosol: reaction products and reversibility of uptake under dark and irradiated conditions, Atmos. Chem. Phys., 9, 3331–3345, doi:10.5194/acp-9-3331-2009, 2009.

Gómez Alvarez, E., Viidanoja, J., Muñoz, A., Wirtz, A., and Hjorth, J.: Experimental confirmation of the dicarbonyl route in the photo-oxidation of toluene and benzene, Environ. Sci. Technol., 41, 8362–8369, doi:10.1021/es0713274, 2007.

Greenblatt, G. D., Orlando, J. J., Burkholder, J. B., and Ravishankara, A. R.: Absorption Measurements of Oxygen Between 330 and 1140 nm, J. Geophys. Res., 95, 18577–18582, doi:10.1029/JD095iD11p18577, 1990.

Grosjean, E., Grosjean, D., Fraser, M. P., and Cass, G. R.: Air quality model evaluation data for organics. 2. C1–C14 Carbonyls in Los Angeles air, Environ. Sci. Technol., 30, 2687–2703, 1996.

Guimbaud, C., Catoire, V., Bergeat, A., Michel, E., Schoon, N., Amelynck, C., Labonnette, D., and Poulet, G.: Kinetics of the reactions of acetone and glyoxal with O$_2^+$ and NO$^+$ ions and

application to the detection of oxygenated volatile organic compounds in the atmosphere by chemical ionization mass spectrometry, Int. J. Mass Spectrom., 263, 276–288, 2007.

Hamilton, J. F., Baeza-Romero, M. T., Finessi, E., Rickard, A. R., Healy, R. M., Peppe, S., Adams, T. J., Daniels, M. J. S., Ball, S. M., Goodall, I. C. A., Monks, P. S., Borras, E., and Munoz, A.: Online and offline mass spectrometric study of the impact of oxidation and ageing on glyoxal chemistry and uptake onto ammonium sulfate aerosols, Faraday Discuss., 165, 447–472, doi:10.1039/C3FD00051F, 2013.

Hennigan, C. J., Bergin, M. H., Russell, A. G., Nenes, A., and Weber, R. J.: Gas/particle partitioning of water-soluble organic aerosol in Atlanta, Atmos. Chem. Phys., 9, 3613–3628, doi:10.5194/acp-9-3613-2009, 2009.

Henry, S. B., Kammrath, A., and Keutsch, F. N.: Quantification of gas-phase glyoxal and methylglyoxal via the Laser-Induced Phosphorescence of (methyl)GLyOxal Spectrometry (LIPGLOS) Method, Atmos. Meas. Tech., 5, 181–192, doi:10.5194/amt-5-181-2012, 2012.

Hermans, C.: Measurement of Absorption Cross Sections and Spectroscopic Molecular Parameters: O$_2$ and its Collisonal Induced Absorption, available at: http://spectrolab.aeronomie.be/data/o4.txt (last access: 18 August 2014), 2010.

Hermans, C., Vandaele, A., Carleer, M., Fally, S., Colin, R., Jenouvrier, A., Coquart, B., and Mérienne, M. F.: Absorption cross-sections of atmospheric constituents: NO$_2$, O$_2$, and H$_2$O, Environ. Sci. Pollut. R., 6, 151–158, 1999.

Ho, S. S. H. and Yu, J. Z.: Feasibility of collection and analysis of airborne carbonyls by on-sorbent derivatization and thermal desorption, Anal. Chem., 74, 1232–1240, 2002.

Huisman, A. J., Hottle, J. R., Coens, K. L., DiGangi, J. P., Galloway, M. M., Kammrath, A., and Keutsch, F. N.: Laser-induced phosphorescence for the in situ detection of glyoxal at part per trillion mixing ratios, Anal. Chem., 80, 5884–5891, 2008.

Huisman, A. J., Hottle, J. R., Galloway, M. M., DiGangi, J. P., Coens, K. L., Choi, W., Faloona, I. C., Gilman, J. B., Kuster, W. C., de Gouw, J., Bouvier-Brown, N. C., Goldstein, A. H., LaFranchi, B. W., Cohen, R. C., Wolfe, G. M., Thornton, J. A., Docherty, K. S., Farmer, D. K., Cubison, M. J., Jimenez, J. L., Mao, J., Brune, W. H., and Keutsch, F. N.: Photochemical modeling of glyoxal at a rural site: observations and analysis from BEARPEX 2007, Atmos. Chem. Phys., 11, 8883–8897, doi:10.5194/acp-11-8883-2011, 2011.

Ieda, T., Kitamori, Y., Mochida, M., Hirata, R., Hirano, T., Inukai, K., Fujinuma, Y., and Kawamura, K.: Diurnal variations and vertical gradients of biogenic volatile and semi-volatile organic compounds at the Tomakomai larch forest station in Japan, Tellus B, 58, 177–186, 2006.

Ip, H. S. S., Huang, X. H. H., and Yu, J. Z.: Effective Henry's law constants of glyoxal, glyoxylic acid, and glycolic acid, Geophys. Res. Lett., 36, L01802, doi:10.1029/2008GL036212, 2009.

Jordan, A., Haidacher, S., Hanel, G., Hartungen, E., Märk, L., Seehauser, H., Schottkowsky, R., Sulzer, P., and Märk, T. D.: A high resolution and high sensitivity proton-transfer-reaction time-of-flight mass spectrometer (PTR-TOF-MS), Int. J. Mass Spectrom., 286, 122–128, 2009.

Kampf, C. J., Waxman, E. M., Slowik, J. G., Dommen, J., Pfaffenberger, L., Praplan, A. P., Prévôt, A. S. H., Baltensperger, U., Hoffmann, T., and Volkamer, R.: Effective Henry's law partition-

ing and the salting constant of glyoxal in aerosols containing sulfate, Environ. Sci. Technol., 47, 4236–4244, 2013.

Karl, T., Guenther, A., Turnipseed, A., Tyndall, G., Artaxo, P., and Martin, S.: Rapid formation of isoprene photo-oxidation products observed in Amazonia, Atmos. Chem. Phys., 9, 7753–7767, doi:10.5194/acp-9-7753-2009, 2009.

Kawamura, K., Okuzawa, K., Aggarwal, S. G., Irie, H., Kanaya, Y., and Wang, Z.: Determination of gaseous and particulate carbonyls (glycolaldehyde, hydroxyacetone, glyoxal, methylglyoxal, nonanal and decanal) in the atmosphere at Mt. Tai, Atmos. Chem. Phys., 13, 5369–5380, doi:10.5194/acp-13-5369-2013, 2013.

Knote, C., Hodzic, A., Jimenez, J. L., Volkamer, R., Orlando, J. J., Baidar, S., Brioude, J., Fast, J., Gentner, D. R., Goldstein, A. H., Hayes, P. L., Knighton, W. B., Oetjen, H., Setyan, A., Stark, H., Thalman, R., Tyndall, G., Washenfelder, R., Waxman, E., and Zhang, Q.: Simulation of semi-explicit mechanisms of SOA formation from glyoxal in aerosol in a 3-D model, Atmos. Chem. Phys., 14, 6213–6239, doi:10.5194/acp-14-6213-2014, 2014.

Langridge, J. M., Ball, S. M., Shillings, A. J. L., and Jones, R. L.: A broadband absorption spectrometer using light emitting diodes for ultrasensitive, in situ trace gas detection, Rev. Sci. Instrum., 79, 123110, doi:10.1063/1.3046282, 2008.

Lee, Y. N., Zhou, X., Kleinman, L. I., Nunnermacker, L. J., Springston, S. R., Daum, P. H., Newman, L., Keigley, W. G., Holdren, M. W., Spicer, C. W., Young, V., Fu, B., Parrish, D. D., Holloway, J., Williams, J., Roberts, J. M., Ryerson, T. B., and Fehsenfeld, F. C.: Atmospheric chemistry and distribution of formaldehyde and several multioxygenated carbonyl compounds during the 1995 Nashville Middle Tennessee Ozone Study, J. Geophys. Res.-Atmos., 103, 22449–22462, 1998.

Matsunaga, S., Mochida, M., and Kawamura, K.: Variation on the atmospheric concentrations of biogenic carbonyl compounds and their removal processes in the northern forest at Moshiri, Hokkaido Island in Japan, J. Geophys. Res.-Atmos., 109, D04302, doi:10.1029/2003JD004100, 2004.

McNeill, V. F., Woo, J. L., Kim, D. D., Schwier, A. N., Wannell, N. J., Sumner, A. J., and Barakat, J. M.: Aqueous-phase secondary organic aerosol and organosulfate formation in atmospheric aerosols: a modeling study, Environ. Sci. Technol., 46, 8075–8081, 2012.

Meller, R., Raber, W., Crowley, J. N., Jenkin, M. E., and Moortgat, G. K.: The UV-visible absorption spectrum of methylglyoxal, J. Photoch. Photobio. A, 62, 163–171, 1991.

Michel, E., Schoon, N., Amelynck, C., Guimbaud, C., Catoire, V., and Arijs, E.: A selected ion flow tube study of the reactions of H_3O^+, NO^+ and O_2^+ with methyl vinyl ketone and some atmospherically important aldehydes, Int. J. Mass Spectrom., 244, 50–59, 2005.

Muñoz, A., Vera, T., Sidebottom, H., Mellouki, A., Borrás, E., Rodenas, M., Clemente, E., and Vazquez, M.: Studies on the atmospheric degradation of chlorpyrifosmethyl, Environ. Sci. Technol., 45, 1880–1886, 2011.

Muñoz, A., Vera, T., Sidebottom, H., Ródenas, M., Borrás, E., Vázquez, M., Raro, M., and Mellouki, A.: Studies on the atmospheric fate of propachlor (2-chloro-Nisopropylacetanilide) in the gas-phase, Atmos. Environ., 49, 33–40, 2012.

Muñoz, A., Vera, T., Ródenas, T., Borrás, E., Mellouki, A., Treacy, J., and Sidebottom, H.: Gas-phase degradation of the herbicide ethalfluralin under atmospheric conditions, Chemosphere, 95, 395–401, 2014.

Myriokefalitakis, S., Vrekoussis, M., Tsigaridis, K., Wittrock, F., Richter, A., Brühl, C., Volkamer, R., Burrows, J. P., and Kanakidou, M.: The influence of natural and anthropogenic secondary sources on the glyoxal global distribution, Atmos. Chem. Phys., 8, 4965–4981, doi:10.5194/acp-8-4965-2008, 2008.

Niki, H., Maker, P. D., Savage, C. M., and Breitenbach, L. P.: An FTIR study of the Cl-atom-initiated reaction of glyoxal, Int. J. Chem. Kinet., 17, 547–558, 1985.

Nozière, B., Dziedzic, P., and Córdova, A.: Products and kinetics of the liquid-phase reaction of glyoxal catalyzed by ammonium ions (NH_4^+), J. Phys. Chem. A, 113, 231–237, 2008.

O'Keefe, A. and Deacon, D. A. G.: Cavity ring-down optical spectrometer for absorption-measurements using pulsed laser sources, Rev. Sci. Instrum., 59, 2544–2551, 1988.

Okuzawa, K., Mochida, M., Bendle, J., Wang, H., and Kawamura, K.: Diurnal variation of semi-volatile dicarbonyls and hydroxycarbonyls in the urban atmosphere, Chikyukagaku (Geochemistry), 41, 125–134, 2007.

Orlando, J. J. and Tyndall, G. S.: Mechanisms for the reactions of OH with two unsaturated aldehydes: crotonaldehyde and acrolein, J. Phys. Chem. A, 106, 12252–12259, 2002.

Osthoff, H. D., Brown, S. S., Ryerson, T. B., Fortin, T. J., Lerner, B. M., Williams, E. J., Pettersson, A., Baynard, T., Dubé, W. P., Ciciora, S. J., and Ravishankara, A. R.: Measurement of atmospheric NO$_2$ by pulsed cavity ring-down spectroscopy, J. Geophys. Res., 111, D12305, doi:10.1029/2005JD006942, 2006.

Pang, X., Lewis, A. C., and Ródenas García, M.: Microfluidic lab-on-a-chip derivatization for gaseous carbonyl analysis, J. Chromatogr. A, 1296, 93–103, 2013.

Pang, X., Lewis, A. C., Rickard, A. R., Baeza-Romero, M. T., Adams, T. J., Ball, S. M., Daniels, M. J. S., Goodall, I. C. A., Monks, P. S., Peppe, S., Ródenas García, M., Sánchez, P., and Muñoz, A.: A smog chamber comparison of a microfluidic derivatisation measurement of gas-phase glyoxal and methylglyoxal with other analytical techniques, Atmos. Meas. Tech., 7, 373–389, doi:10.5194/amt-7-373-2014, 2014.

Profeta, L. T. M., Sams, R. L., Johnson, T. J., and Williams, S. D.: Quantitative infrared intensity studies of vapor-phase glyoxal, methylglyoxal, and 2,3-butanedione (diacetyl) with vibrational assignments, J. Phys. Chem. A, 115, 9886–9900, 2011.

Raber, W.: Zur Photooxidation einiger atmosphaerischer Spurengase in Luft: die Carbonylverbindungen Methylethylketon, Methylvinylketon, Methacrolein und Methylglyoxal, PhD thesis, J. Gutenberg University, Mainz, 1992.

Rodenas, M.: Improvements in Spectroscopy Data Processing: Faster Production and Better Reliability of Laboratory Data, Report for ESF-INTROP Exchange Grants, available at: http://www.ceam.es/GVAceam/archivos/MRodenasINTROPReport.pdf (last access: 18 August 2014), 2008.

Rothman, L. S., Gordon, I. E., Barbe, A., Benner, D. C., Bernath, P. F., Birk, M., Boudon, V., Brown, L. R., Campargue, A., Champion, J. P., Chance, K., Coudert, L. H., Dana, V., Devi, V. M., Fally, S., Flaud, J. M., Gamache, R. R., Goldman, A., Jacquemart, D., Kleiner, I., Lacome, N., Lafferty, W. J., Mandin, J. Y., Massie, S. T., Mikhailenko, S. N., Miller, C. E.,

Moazzen-Ahmadi, N., Naumenko, O. V., Nikitin, A. V., Orphal, J., Perevalov, V. I., Perrin, A., Predoi-Cross, A., Rinsland, C. P., Rotger, M., Simeckov, M., Smith, M. A. H., Sung, K., Tashkun, S. A., Tennyson, J., Toth, R. A., Vandaele, A. C., and Vander Auwera, J.: The HITRAN 2008 molecular spectroscopic database, J. Quant. Spectrosc. Ra., 110, 533–572, 2009.

Rothman, L., Gordon, I., Barber, R., Dothe, H., Gamache, R., Goldman, A., Perevalov, V., Tashkun, S., and Tennyson, J.: HITEMP, the high-temperature molecular spectroscopic database, J. Quant. Spectrosc. Ra., 111, 2139–2150, 2010.

Rothman, L. S., Gordon, I. E., Babikov, Y., Barbe, A., Chris Benner, D., Bernath, P. F., Birk, M., Bizzocchi, L., Boudon, V., Brown, L. R., Campargue, A., Chance, K., Cohen, E. A., Coudert, L. H., Devi, V. M., Drouin, B. J., Fayt, A., Flaud, J. M., Gamache, R. R., Harrison, J. J., Hartmann, J. M., Hill, C., Hodges, J. T., Jacquemart, D., Jolly, A., Lamouroux, J., Le Roy, R. J., Li, G., Long, D. A., Lyulin, O. M., Mackie, C. J., Massie, S. T., Mikhailenko, S., Müller, H. S. P., Naumenko, O. V., Nikitin, A. V., Orphal, J., Perevalov, V., Perrin, A., Polovtseva, E. R., Richard, C., Smith, M. A. H., Starikova, E., Sung, K., Tashkun, S., Tennyson, J., Toon, G. C., Tyuterev, V. G., and Wagner, G.: The HITRAN2012 molecular spectroscopic database, J. Quant. Spectrosc. Ra., 130, 4–50, doi:10.1016/j.jqsrt.2013.07.002, 2013.

Ryerson, T. B., Andrews, A. E., Angevine, W. M., Bates, T. S., Brock, C. A., Cairns, B., Cohen, R. C., Cooper, O. R., de Gouw, J. A., Fehsenfeld, F. C., Ferrare, R. A., Fischer, M. L., Flagan, R. C., Goldstein, A. H., Hair, J. W., Hardesty, R. M., Hostetler, C. A., Jimenez, J. L., Langford, A. O., McCauley, E., McKeen, S. A., Molina, L. T., Nenes, A., Oltmans, S. J., Parrish, D. D., Pederson, J. R., Pierce, R. B., Prather, K., Quinn, P. K., Seinfeld, J. H., Senff, C. J., Sorooshian, A., Stutz, J., Surratt, J. D., Trainer, M., Volkamer, R., Williams, E. J., and Wofsy, S. C.: The 2010 California research at the Nexus of air quality and climate change (CalNex) field study, J. Geophys. Res., 5830–5866, doi:10.1002/jgrd.50331, 2013.

Shetter, R. E., Davidson, J. A., Cantrell, C. A., and Calvert, J. G.: Temperature variable long path cell for absorption-measurements, Rev. Sci. Instrum., 58, 1427–1428, 1987.

Siese, M. and Zetzsch, C.: Addition of OH to Acetylene and Consecutive Reactions of the Adduct with O$_2$, Zeitschrift für Physikalische Chemie, 188, 1–2, 75–89, doi:10.1524/zpch.1995.188.Part_1_2.075, 1995.

Sinreich, R., Volkamer, R., Filsinger, F., Frieß, U., Kern, C., Platt, U., Sebastián, O., and Wagner, T.: MAX-DOAS detection of glyoxal during ICARTT 2004, Atmos. Chem. Phys., 7, 1293–1303, doi:10.5194/acp-7-1293-2007, 2007.

Sinreich, R., Coburn, S., Dix, B., and Volkamer, R.: Ship-based detection of glyoxal over the remote tropical Pacific Ocean, Atmos. Chem. Phys., 10, 11359–11371, doi:10.5194/acp-10-11359-2010, 2010.

Stavrakou, T., Müller, J.-F., De Smedt, I., Van Roozendael, M., Kanakidou, M., Vrekoussis, M., Wittrock, F., Richter, A., and Burrows, J. P.: The continental source of glyoxal estimated by the synergistic use of spaceborne measurements and inverse modelling, Atmos. Chem. Phys., 9, 8431–8446, doi:10.5194/acp-9-8431-2009, 2009.

Talukdar, R. K., Zhu, L., Feierabend, K. J., and Burkholder, J. B.: Rate coefficients for the reaction of methylglyoxal (CH3COCHO) with OH and NO$_3$ and glyoxal (HCO)$_2$ with

NO$_3$, Atmos. Chem. Phys., 11, 10837–10851, doi:10.5194/acp-11-10837-2011, 2011.

Thalman, R.: Development of Cavity Enhanced Differential Optical Absorption Spectroscopy (CE-DOAS) and application to laboratory and field measurements of trace gases and aerosols, PhD dissertation, University of Colorado, Boulder, USA, 235 pp., 2013.

Thalman, R. and Volkamer, R.: Inherent calibration of a blue LED-CE-DOAS instrument to measure iodine oxide, glyoxal, methyl glyoxal, nitrogen dioxide, water vapour and aerosol extinction in open cavity mode, Atmos. Meas. Tech., 3, 1797–1814, doi:10.5194/amt-3-1797-2010, 2010.

Thalman, R., Zarzana, K. J., Tolbert, M. A., and Volkamer, R.: Rayleigh scattering cross-section measurements of nitrogen, argon, oxygen and air, J. Quant. Spectrosc. Ra., 147, 171–177, 2014.

Topping, D., Connolly, P., and McFiggans, G.: Cloud droplet number enhanced by co-condensation of organic vapours, Nat. Geosci., 6, 443–446, 2013.

Tuazon, E. C. and Atkinson, R.: A product study of the gas-phase reaction of isoprene with the OH radical in the presence of NO$_x$, Int. J. Chem. Kinet., 22, 1221–1236, 1990a.

Tuazon, E. C. and Atkinson, R.: A product study of the gas-phase reaction of Methacrolein with the OH radical in the presence of NO$_x$, Int. J. Chem. Kinet., 22, 591–602, 1990b.

Vandaele, A. C., Hermans, C., Fally, S., Carleer, M., Colin, R., Merienne, M. F., Jenouvrier, A., and Coquart, B.: High-resolution Fourier transform measurement of the NO$_2$ visible and near-infared absorption cross sections: temperature and pressure effects, J. Geophys. Res., 107, 4348, doi:10.1029/2001JD000971, 2002.

Volkamer, R., Molina, L. T., Molina, M. J., Shirley, T., and Brune, W. H.: DOAS measurement of glyoxal as an indicator for fast VOC chemistry in urban air, Geophys. Res. Lett., 32, L08806, doi:10.1029/2005GL022616, 2005a.

Volkamer, R., Spietz, P., Burrows, J., and Platt, U.: High-resolution absorption cross-section of glyoxal in the UV-vis and IR spectral ranges, J. Photoch. Photobio. A, 172, 35–46, 2005b.

Volkamer, R., San Martini, F., Molina, L. T., Salcedo, D., Jimenez, J. L., and Molina, M. J.: A missing sink for gas-phase glyoxal in Mexico City: formation of secondary organic aerosol, Geophys. Res. Lett., 34, L19807, doi:10.1029/2007GL030752, 2007.

Volkamer, R., Ziemann, P. J., and Molina, M. J.: Secondary Organic Aerosol Formation from Acetylene (C$_2$H$_2$): seed effect on SOA yields due to organic photochemistry in the aerosol aqueous phase, Atmos. Chem. Phys., 9, 1907–1928, doi:10.5194/acp-9-1907-2009, 2009.

Volkamer, R., Baidar, S., Campos, T. L., Coburn, S., DiGangi, J. P., Dix, B., Koenig, T. K., Ortega, I., Pierce, B. R., Reeves, M., Sinreich, R., Wang, S., Zondlo, M. A., and Romashkin, P. A.: Aircraft measurements of bromine monoxide, iodine monoxide, and glyoxal profiles in the tropics: comparison with ship-based and in situ measurements, Atmos. Meas. Tech. Discuss., 8, 623–687, doi:10.5194/amtd-8-623-2015, 2015.

Washenfelder, R. A., Langford, A. O., Fuchs, H., and Brown, S. S.: Measurement of glyoxal using an incoherent broadband cavity enhanced absorption spectrometer, Atmos. Chem. Phys., 8, 7779–7793, doi:10.5194/acp-8-7779-2008, 2008.

Washenfelder, R. A., Young, C. J., Brown, S. S., Angevine, W. M., Atlas, E. L., Blake, D. R., Bon, D. M., Cubison, M. J., de Gouw, J. A., Dusanter, S., Flynn, J., Gilman, J. B., Graus, M., Griffith, S., Grossberg, N., Hayes, P. L., Jimenez, J. L., Kuster, W. C., Lefer, B. L., Pollack, I. B., Ryerson, T. B., Stark, H., Stevens, P. S., and Trainer, M. K.: The glyoxal budget and its contribution to organic aerosol for Los Angeles, California, during CalNex 2010, J. Geophys. Res., 116, D00V02, doi:10.1029/2011JD016314, 2011.

Waxman, E. M., Dzepina, K., Ervens, B., Lee-Taylor, J., Aumont, B., Jimenez, J. L., Madronich, S., and Volkamer, R.: Secondary organic aerosol formation from semi- and intermediate-volatility organic compounds and glyoxal: relevance of O/C as a tracer for aqueous multiphase chemistry, Geophys. Res. Lett., 40, 978–982, 2013.

Wyche, K. P., Blake, R. S., Ellis, A. M., Monks, P. S., Brauers, T., Koppmann, R., and Apel, E. C.: Technical Note: Performance of Chemical Ionization Reaction Time-of-Flight Mass Spectrometry (CIR-TOF-MS) for the measurement of atmospherically significant oxygenated volatile organic compounds, Atmos. Chem. Phys., 7, 609–620, doi:10.5194/acp-7-609-2007, 2007.

Yu, J., Jeffries, H. E., and Sexton, K. G.: Atmospheric photooxidation of alkylbenzenes – I. Carbonyl product analyses, Atmos. Environ., 31, 2261–2280, 1997.

Yu, G., Bayer, A. R., Galloway, M. M., Korshavn, K. J., Fry, C. G., and Keutsch, F. N.: Glyoxal in aqueous ammonium sulfate solutions: products, kinetics and hydration effects, Environ. Sci. Technol., 45, 6336–6342, 2011.

Zalicki, P. and Zare, R. N.: Cavity ring-down spectroscopy for quantitative absorption-measurements, J. Chem. Phys., 102, 2708–2717, 1995.